2

Distribution

Category UC-70

HYDROLOGY DOCUMENT NUMBER 175

SAND82-1434
Unlimited Release
Printed April 1985

Bulk and Thermal Properties of the Functional Tuffaceous Beds in Holes USW G-1, UE-25a#1, and USW G-2, Yucca Mountain, Nevada

Allen R. Lappin
Earth Sciences Division
and
Francis B. Nimick
NNWSI Geotechnical Projects Division

Sandia National Laboratories
Albuquerque, NM 87185

ABSTRACT

One emplacement horizon considered for a nuclear-waste repository at Yucca Mountain, Nevada, adjacent to the Nevada Test Site, consists of a zeolitized section. This section is defined here as an informal functional unit called the Tuffaceous Beds. This report describes the logic, data, and uncertainties involved in picking the boundaries of the functional unit in exploratory Holes USW G-1, UE-25a#1, and USW G-2. It also includes frequency profiles for grain density and porosity within the unit in the three exploratory holes. Results indicate that the functional Tuffaceous Beds range from 143 to 312 m in total thickness in the three holes studied. Unit-wide average grain densities and porosities of nonwelded ash-flows are 2.39 g/cm^3 and 0.33, respectively. The average matrix thermal conductivity of heavily zeolitized tuffs is constant at 1.95 W/m•K. This value leads to average estimated conductivities of saturated and dehydrated nonwelded ashflows within the functional Tuffaceous Beds of 1.3 and 0.9 W/m•K, respectively. Available confined measurements indicate an average predehydration linear-expansion coefficient of 6.7 x 10^{-6} K^{-1}; individual values range from 2.8 to 13.2 x 10^{-6} K^{-1}. Transdehydration expansion behavior is variable, with average coefficients ranging from -56 to -29 x 10^{-6} K^{-1}, depending on relative zeolite and (quartz + feldspar) contents. Postdehydration behavior is also sensitive to mineralogy, with average unconfined coefficients ranging from -4.5 to +7.8 x 10^{-6} K^{-1} for the different subunits within the functional Tuffaceous Beds. For the nonwelded ashflows dominant within the unit, pre-, trans-, and postdehydration expansion coefficients of +6.7, -56, and -4.5 x 10^{-6} K^{-1} are most representative.

CONTENTS

	Page
Introduction	1
Functional Definition and Boundaries of Unit	1
Frequency Distributions of Grain Density and Porosity	6
Thermal Conductivity	20
Thermal Expansion	27
Summary	40
Appendix: Detailed Data and Uncertainties in Picking the Upper and Lower Boundaries of the Functional Tuffaceous Beds	44
References	54

FIGURES

Figure		Page
1.	Location Map	2
2.	Stratigraphy of Tuff Units at Yucca Mountain	3
3.	Cumulative Frequency Diagram of Grain Density	18
4.	Cumulative Frequency Diagram of Porosity	19
5.	Grain Density Versus Matrix Thermal Conductivity	23
6.	Cumulative Frequency Diagram of Matrix Thermal Conductivity	24
7.	Schematic Representation of Thermal Expansion Behavior in the Functional Tuffaceous Beds	39

LIST OF TABLES

Table		Page
1.	Summary of Elevations, Thicknesses, and Average Bulk Properties	5
2.	Extrapolated Bulk Properties for the Functional Tuffaceous Beds in USW G-1	8
3.	Extrapolated Bulk Properties for the Functional Tuffaceous Beds in UE-25a#1	10
4.	Extrapolated Bulk Properties for the Functional Tuffaceous Beds in USW G-2	12
5.	Cumulative Frequencies of Independent Parameters, Functional Tuffaceous Beds in USW G-1	14
6.	Cumulative Frequencies of Independent Parameters, Functional Tuffaceous Beds in UE-25a#1	15
7.	Cumulative Frequencies of Independent Parameters, Functional Tuffaceous Beds in USW G-2	16
8.	Summary of Thermal Conductivity Measurements of Heavily Zeolitized Tuffs	22
9.	Cumulative Frequency of Theoretical Matrix Conductivity of Strongly Zeolitized Tuffs	25
10.	Linear Thermal Expansion of Zeolitized Tuffs	32
11.	Summary of Contractions Relative to Initial Length During Unconfined Linear Expansion Measurements on Heavily Zeolitized Tuffs	34
12.	Estimated Linear Thermal Expansion of Rock Types Within the Functional Tuffaceous Beds in USW G-1, UE-25a#1, and USW G-2	38

INTRODUCTION

The Nevada Nuclear Waste Storage Investigations (NNWSI) project administered by the Nevada Operations Office of the US Department of Energy (DOE), is investigating the feasibility of emplacing commercial high-level nuclear wastes underground at Yucca Mountain on and near the Nevada Test Site (NTS) (Figure 1). As part of the investigations, an evaluation was made of the relative merits of four tuff units at Yucca Mountain as candidate horizons for waste emplacement.[1] The objective of this report is to document bulk and thermal property data used in evaluating one of the four units, the Tuffaceous Beds of Calico Hills. Average thermal properties, vertical distributions of bulk properties within the Tuffaceous Beds, and estimated uncertainties in all measurements are defined. The final result is an estimate of lateral and vertical variability. Since only data received as of March 15, 1982, are included here, the discussion is limited to exploratory holes USW G-1, UE-25a#1, and USW G-2 (Figure 1).

FUNCTIONAL DEFINITION AND BOUNDARIES OF UNIT

Figure 2 shows the general stratigraphy of tuff units at Yucca Mountain. The Tuffaceous Beds of Calico Hills consist of many nonwelded ashflows and thin interbeds of bedded/reworked tuff. There is usually a relatively thick zone of bedded/reworked tuff and tuffaceous sandstone at the base of the unit.[2,3]

From a thermal and mechanical point of view, the dominant feature of the unit is its pervasive zeolitization. Using zeolitization as a prime characteristic, a functional unit can also be defined, which in this report is called the functional Tuffaceous Beds. This unit is thicker than the formal stratigraphic unit. It includes the lower zeolitized ashflow tuff in the overlying Topopah Spring Member of the Paintbrush Tuff and the zeolitized upper portion of the ashflow tuffs in the underlying Prow Pass Member of the Crater Flat Tuff. Defined in this way, the functional Tuffaceous Beds are more complex and thicker than the ashflow portions of the Tuffaceous Beds of Calico Hills.

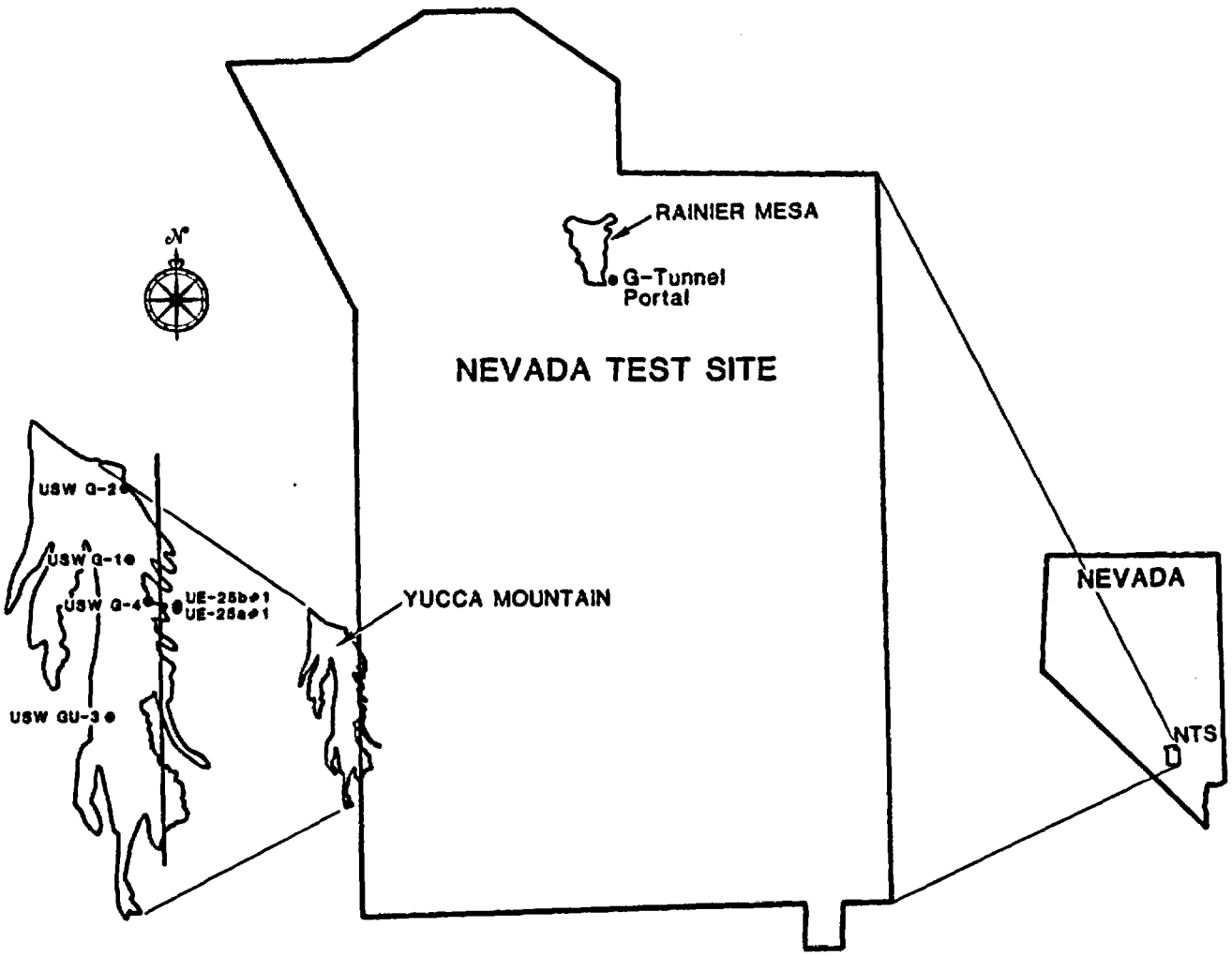

Figure 1. Location Map

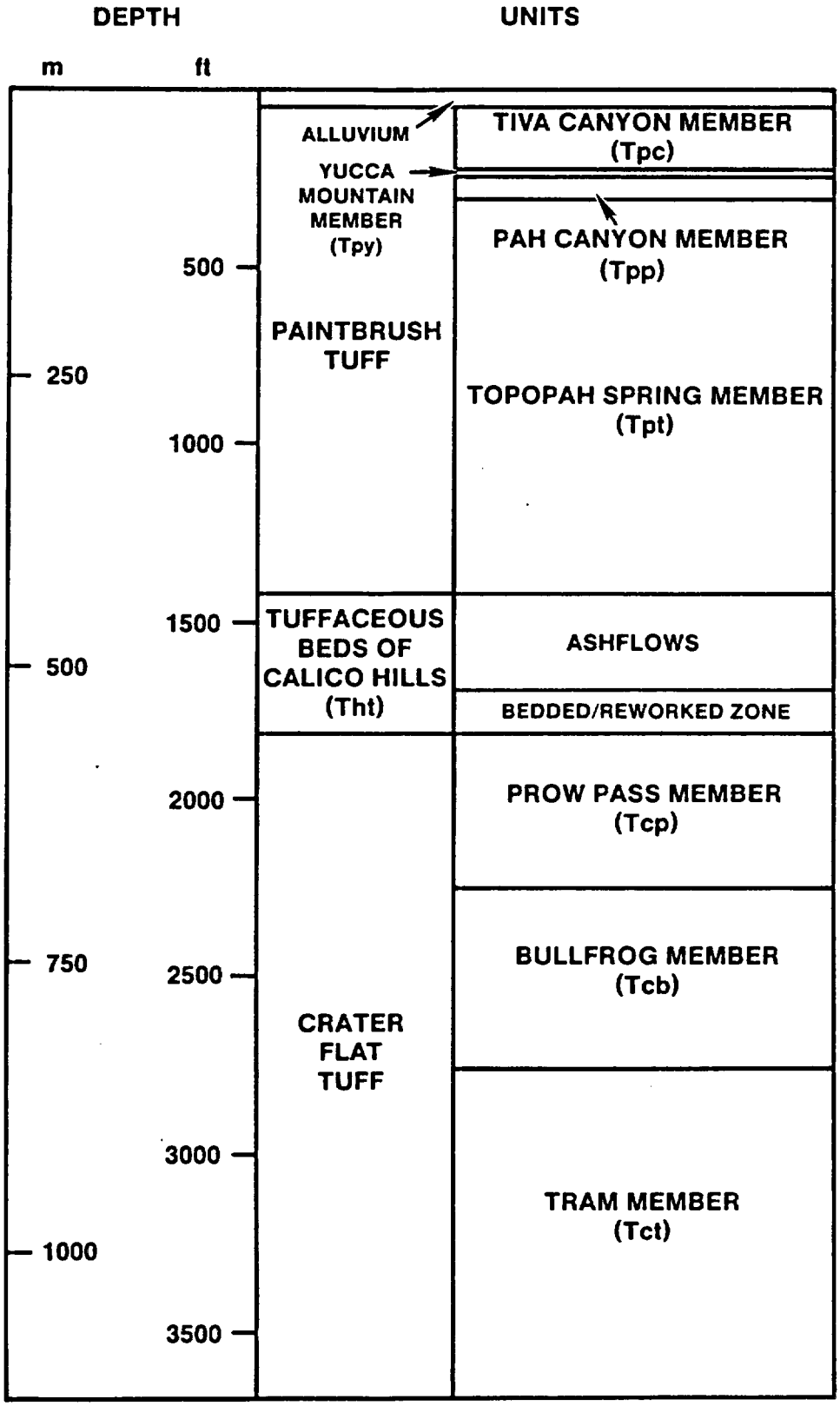

Figure 2. Stratigraphy of Tuff Units at Yucca Mountain

In the summary data tables in this report, three separate portions of the functional Tuffaceous Beds are usually distinguished in an effort to evaluate variability within the expanded unit. The three subunits are defined as follows: (1) from the top of zeolitization in the Topopah Spring Member to the base of the ashflow portion of the Tuffaceous Beds of Calico Hills, (2) from the top to the bottom of the basal bedded/reworked zone of the Tuffaceous Beds of Calico Hills, and (3) from the top of the Prow Pass Member to the top of the first devitrified zone in the Prow Pass Member. The upper of the three subunits was originally considered as a candidate emplacement horizon.

In this section, the overall character of the functional Tuffaceous Beds in each of the exploratory holes from which data were available as of March 15, 1982, is summarized. The Appendix contains a detailed discussion of the picks made in each hole. Four sources of data were used to distinguish the functional Tuffaceous Beds from adjacent units and to identify the subunits within the Tuffaceous Beds: (1) lithologic logs, (2) mineralogical analyses, (3) downhole density logs, and (4) bulk-property measurements. It appears that zonal boundaries can be defined consistently within this functional unit, with limited uncertainties, as a result of sample spacings and required extrapolations. Boundaries usually are picked to coincide as closely as possible with the apparent mineralogical zonation because of the mineralogical control of thermal expansion and thermal conductivity.

Table 1 summarizes measured bulk properties, estimated thicknesses, and elevations within the various subunits as well as for the functional unit as a whole. As shown, overall unit thickness ranges from 143 m in USW G-1 to 312 m in USW G-2. The thickness of the upper subunit, consisting largely of the nonwelded ashflows within the Tuffaceous Beds of Calico Hills, ranges from 104 to 312 m. If the portion of this subunit within the Topopah Spring Member is excluded, thickness ranges from 95 to 289 m. Average grain densities in the upper subunit range from 2.37 to 2.43 g/cm^3; average porosities from 0.30 to 0.35.

Uncertainties in the position of the upper and lower boundaries of the functional unit range from ~1 to >10 m. The full four sets of data are

Table 1

Summary of Elevations, Thicknesses, and Average Bulk Properties of the Functional Tuffaceous Beds in USW G-1, UE-25a#1, and USW G-2

	Elevation (m)*	Thickness (m)*	Grain Density (g/cm^3)	Total Porosity
USW G-1				
Total Unit	757.2 to 900.5	143.3	2.43 (38)	0.35
Subunit a**	796.3 to 900.5	104.2	2.40 (28)	0.36
Subunit b	776.4 to 796.3	19.9	2.56 (6)	0.30
Subunit c	757.2 to 776.4	19.2	2.41 (4)	0.36
UE-25a#1				
Total Unit	636.8 to 796.9	160.1	2.37 (28)	0.30
Subunit a	653.9 to 796.9	143.0	2.36 (25)	0.31
Subunit b	639.6 to 653.9	14.3	2.47 (2)	0.20
Subunit c	636.8 to 639.6	2.8	2.37 (1)	0.21
USW G-2				
Total Unit	729.7 to 1041.8	312.1	2.40 (48)	0.31
Subunit a	729.7 to 1041.8	312.1	2.40 (48)	0.31
Subunit b	Faulted Out			
Subunit c	Faulted Out			

*: Not corrected for drill hole deviation.

**: See text for description of subunits.

( ): Numbers of samples analyzed for bulk properties.

available. They are necessary only for these contacts. The central part of the unit (the basal bedded/reworked portion of the Tuffaceous Beds of Calico Hills) is defined solely on the basis of the lithologic logs. Given the distinctive textural nature of bedded/reworked tuffs, this should involve no appreciable uncertainty other than that resulting from hole deviation and possibly from incomplete core recovery.

Note that bulk properties reported in Table 1 are averages of measured values rather than estimated averages for the zone and subzones as a whole. Many of the samples for which bulk properties are available were analyzed as part of thermomechanical studies and thus represent irregular intervals through the unit. Averages listed in Table 1 therefore might not be representative of the functional Tuffaceous Beds as a whole. This problem is addressed in the following section.

FREQUENCY DISTRIBUTIONS OF GRAIN DENSITY AND POROSITY

Previous work[4,5] has indicated that the thermal conductivity and the mechanical properties of silicic tuffs are a function of porosity and mineralogy. Measurements of grain density form a basis for extrapolating mineralogical results, although the linkage of grain density with mineralogical variation is not always unique. Porosity in tuffs is likewise inversely related to the degree of welding. This relationship has inherent ambiguities because of secondary pore-filling processes such as zeolitization and/or vapor-phase activity. Data on grain density and on total porosity appear to be adequate for estimating of thermal properties. In the case of thermal expansion and especially of mechanical properties, characterization may require more detailed analysis of mineralogy and fabric--independent of total porosity. Here, however, thermal and mechanical properties are assumed to vary as a function of total porosity and are assumed to be constant for a given porosity over a given range of grain density.

This section lists cumulative frequency distributions for grain density and porosity within the functional Tuffaceous Beds. Frequency-distribution data for these variables have served as primary input to sensitivity analyses relating predicted excavation stability to variations in tuff properties. These analyses have in turn been used to evaluate the functional Tuffaceous Beds as a potential repository horizon[1] and to determine the level of detail at which variables should be understood. The "Latin hypercube" technique[6] proposed for these analyses was used previously in studies related to the disposal of nuclear waste.

The process used to develop frequency data presented here was straightforward. Since it was decided that at least 30 individual sampling points were required across the overall functional Tuffaceous Beds, calculation intervals were chosen to estimate properties at 30 or more evenly spaced depths. Properties at each depth were assumed to be a linear extrapolation of those from overlying and underlying samples. Calculated bulk properties for the functional Tuffaceous Beds in USW G-1, UE-25a#1, and USW G-2 are detailed in Tables 2, 3, and 4, respectively. Corresponding cumulative frequencies of grain densities and porosities are listed in Tables 5-7.

Some explanation of Tables 2-4 is in order. The left-hand column specifies the evenly spaced depths at which bulk properties were calculated. Depths listed in Column 1 are those of the nearest sample for which data are available above the extrapolated depth. At or near the top of the zone, however, an overlying sample was generally not used since it would lie in an entirely different zone. The same consideration occasionally affects extrapolation within the functional Tuffaceous Beds. For example (Table 2), the basal bedded/reworked zone in the Tuffaceous Beds of Calico Hills in USW G-1 extends from 1736 to 1802 ft depth. To reflect this zonation, bulk properties at a depth of 1800 ft were assumed identical to those of a sample in the bedded/reworked zone, at 1792 ft. Analogously, properties at 1815 and 1830 ft were assumed identical to those of the nearest underlying sample in the lowermost ashflow portion of the zone, at 1832 ft. Gaps in Tables 2-4

Table 2

Extrapolated Bulk Properties for the Functional Tuffaceous Beds in USW G-1

Interval: Depths of from 1395 to 1865 ft. in 15-ft increments; n = 32

Extrapolated Depth (ft)	1	2	3	4	5	6	7	8	9	10	11	12	13	14
1395			1396	1		2.44				2.44				0.35
1410	1396	14	1443	33	2.44	2.51	0.07	47	0.298	2.46	0.35	0.39	0.04	0.36
1425	1396	29	1443	18	2.44	2.51	0.07	47	0.383	2.48	0.35	0.39	0.04	0.37
1440	1396	44	1443	3	2.44	2.51	0.07	47	0.064	2.51	0.35	0.39	0.04	0.39
1455	1451	4	1470	15	2.42	2.41	0.01	19	0.211	2.42	0.39	0.37	0.02	0.39
1470	1470	0			2.41		0			2.41	0.37			0.37
1485	1470	15	1489	4	2.41	2.50	0.09	19	0.211	2.48	0.37	0.40	0.03	0.39
1500	1489	11	1504(2)	4	2.50	2.38	0.12	15	0.267	2.41	0.40	0.35	0.05	0.36
1515	1515(3)	0			2.40					2.40	0.33			0.33
1530	1521	9	1552(2)	22	2.49	2.39	0.10	31	0.290	2.46	0.39	0.39	0	0.39
1545	1521	24	1552(2)	7	2.49	2.39	0.10	31	0.226	2.41	0.39	0.39	0	0.39
1560	1552(2)	8	1571	11	2.39	2.40	0.01	19	0.421	2.39	0.39	0.39	0	0.39
1575	1571	4	1596	21	2.40	2.38	0.02	25	0.160	2.40	0.39	0.40	0.01	0.39
1590	1571	19	1596	6	2.40	2.38	0.02	25	0.240	2.38	0.39	0.40	0.01	0.40
1605	1596	9	1606	1	2.38	2.30	0.08	10	0.100	2.31	0.40	0.33	0.07	0.34
1620	1620	0			2.43					2.43	0.36			0.36
1635	1620	15	1652	17	2.43	2.36	0.07	32	0.469	2.40	0.36	0.35	0.01	0.36
1650	1620	30	1652	2	2.43	2.36	0.07	32	0.063	2.36	0.36	0.35	0.01	0.35
1665	1664	1	1668(3)	3	2.45	2.43	0.02	4	0.250	2.44	0.33	0.37	0.04	0.34
1680	1668(3)	12	1706	26	2.43	2.33	0.12	38	0.316	2.39	0.37	0.33	0.04	0.36
1695	1668(3)	27	1706	11	2.43	2.33	0.12	38	0.289	2.37	0.37	0.33	0.04	0.34
1710	1706	4	1722(2)	12	2.33	2.47	0.14	16	0.250	2.37	0.33	0.37	0.04	0.34
1725	1722(2)	3	1743	18	2.47	2.61	0.14	21	0.143	2.49	0.37	0.36	0.01	0.37
1740	1772(2)	18	1743	3	2.47	2.61	0.14	21	0.143	2.59	0.37	0.36	0.01	0.36
1755	1743	12	1763	8	2.61	2.43	0.18	20	0.4	2.50	0.36	0.37	0.01	0.37
1770	1763	7	1773	3	2.43	2.52	0.09	10	0.3	2.49	0.37	0.27	0.10	0.30
1785	1785(2)	0			2.64					2.64	0.27			0.27
1800	1792	8			2.53					2.53	0.24			0.24
1815			1832	17		2.38			1.000	2.38		0.36		0.36
1830			1832	2		2.38			1.000	2.38		0.36		0.36
1845	1832	12	1847(2)	2	2.38	2.44	0.06	14	0.143	2.43	0.36	0.37	0.01	0.37
1860	1847	13	1886	26	2.44	2.59	0.15	39	0.333	2.49	0.37	0.32	0.05	0.35
										2.44±0.07				0.36±0.04

( ): Number of samples analyzed.

Table 2 (Cont'd.)

Legend

1. Depth of closest bulk-property measurements above extrapolated depth.

2. Difference in depth between sample in Column 1 and extrapolated depth.

3. Depth of closest bulk-property measurement below extrapolated depth.

4. Difference in depth between sample in Column 3 and extrapolated depth.

5,6. Reported grain density (g/cm^3) at depths above and below extrapolated depth, respectively.

7. Difference between grain densities in Columns 5 and 6.

8. Total distance (feet) between analyzed samples (Column 2 + Column 4).

9. Smallest value of Columns 2 and 4, divided by value in Column 8.

10. Calculated grain density (g/cm^3) at extrapolated depth.

11.12. Reported porosities at depth given in Columns 1 and 3, respectively.

13. Difference between Columns 11 and 12.

14. Calculated porosity at extrapolated depth.

Table 3

Extrapolated Bulk Properties for the Functional Tuffaceous Beds in UE-25a#1

Interval: Depths of from 1320 to 1845 ft. in 15-ft increments; n = 32

Extrapolated Depth (ft)	1	2	3	4	5	6	7	8	9	10	11	12	13	14
1320			1370	50		2.36				2.36				0.23*1
1335			1370	35		2.36				2.36				0.34*1
1350			1370	20		2.36				2.36				0.22*1
1365			1370	5		2.36				2.36		0.31		0.31
1380	1370	10	1382	2	2.36	2.39	0.03	12	0.167	2.38	0.31	0.36	0.05	0.35
1395	1382	13	1414	19	2.39	2.36	0.03	32	0.406	2.38	0.36	0.36	0.05	0.34
1410	1382	28	1414	4	2.39	2.36	0.03	32	0.125	2.36	0.36	0.31	0.05	0.32
1425	1414	11	1427	2	2.36	2.37	0.01	13	0.154	2.37	0.31	0.32	0.01	0.32
1440	1427	13	1448	8	2.37	2.40	0.03	21	0.381	2.39	0.32	0.34	0.02	0.33
1455	1448	7	1472	17	2.40	2.43	0.03	24	0.292	2.41	0.34	0.33	0.01	0.34
1470	1448	22	1472	2	2.40	2.43	0.03	24	0.083	2.43	0.34	0.33	0.01	0.33
1485	1472	13	1490	5	2.43	2.42	0.01	18	0.278	2.42	0.33	0.28	0.05	0.29
1500	1490	10	1555	55	2.42	2.46	0.04	65	0.154	2.43	0.28	0.33	0.05	0.29
1515	1490	25	1555	40	2.42	2.46	0.04	65	0.385	2.44	0.28	0.33	0.05	0.30
1530	1490	40	1555	25	2.42	2.46	0.04	65	0.385	2.44	0.28	0.33	0.05	0.31
1545	1490	55	1555	10	2.42	2.46	0.04	65	0.154	2.45	0.28	0.33	0.05	0.32
1560	1555	5	1561	1	2.46	2.48	0.02	6	0.167	2.46	0.33	0.34	0.01	0.34
1575	1561	14	1605	30	2.48	2.37	0.11	44	0.318	2.44	0.34	0.30	0.04	0.33
1590	1561	29	1605	15	2.48	2.37	0.11	44	0.341	2.41	0.34	0.30	0.04	0.31
1605	1605	0			2.37					2.37	0.30			0.30
1620	1605	15	1662	42	2.37	2.38	0.01	57	0.263	2.37	0.30	0.35	0.05	0.31
1635	1605	30	1662	27	2.37	2.38	0.01	57	0.474	2.38	0.30	0.35	0.05	0.33
1650	1605	45	1662	12	2.37	2.38	0.01	57	0.211	2.38	0.30	0.35	0.05	0.34
1665	1662	3	1673	8	2.38	2.42	0.04	11	0.273	2.39	0.35	0.39	0.04	0.36
1680	1673	7	1760	80	2.42	2.38	0.04	87	0.080	2.42	0.39	0.25	0.14	0.39
1695	1673	22	1760	65	2.42	2.38	0.04	87	0.253	2.41	0.39	0.25	0.14	0.35
1710	1673	37	1760	50	2.42	2.38	0.04	87	0.425	2.40	0.39	0.25	0.14	0.33
1725	1673	52	1760	35	2.42	2.38	0.04	87	0.402	2.40	0.39	0.25	0.14	0.31
1740	1673	67	1760	20	2.42	2.38	0.04	87	0.230	2.39	0.39	0.25	0.14	0.28
1755	1673	82	1760	5	2.42	2.38	0.04	87	0.057	2.38	0.39	0.25	0.14	0.26
1770	1760	10	1815	45	2.38	2.47	0.09	55	0.182	2.40	0.25	0.26	0.01	0.25
1785	1760	25	1815	30	2.38	2.47	0.09	55	0.455	2.42	0.25	0.26	0.01	0.25
1800	1760	40	1815	15	2.38	2.47	0.09	55	0.273	2.44	0.25	0.26	0.01	0.26
1815	1815	0			2.47					2.47	0.26			0.26
1830	1815	15								2.63*2				0.27
1845	1815	30			2.47					2.47	0.40*3			0.40
										2.41±0.05				0.31±0.04

*1Estimated porosities, based on downhole density log (noncompensated) and assumed grain density.
*2Estimated grain density and porosity assumed same as for tuffaceous sandstone in USW G-1.
*3Estimated, based on presence of sharp low-density zone in downhole log.

Table 3 (Cont'd.)

Legend

1. Depth of closest bulk-property measurements above extrapolated depth.

2. Difference in depth between sample in Column 1 and extrapolated depth.

3. Depth of closest bulk-property measurement below extrapolated depth.

4. Difference in depth between sample in Column 3 and extrapolated depth.

5,6. Reported grain density (g/cm^3) at depths above and below extrapolated depth, respectively.

7. Difference between grain densities in Columns 5 and 6.

8. Total distance (feet) between analyzed samples (Column 2 + Column 4).

9. Smallest value of Columns 2 and 4, divided by value in Column 8.

10. Calculated grain density (g/cm^3) at extrapolated depth.

11.12. Reported porosities at depth given in Columns 1 and 3, respectively.

13. Difference between Columns 11 and 12.

14. Calculated porosity at extrapolated depth.

Table 4

Extrapolated Bulk Properties for the Functional Tuffaceous Beds in USW G-2

Interval: Depths of from 1680 to 2704 ft. in 30-ft increments; n = 32

Extrapolated Depth (ft)	1	2	3	4	5	6	7	8	9	10	11	12	13	14
1760			1768	8		2.37				2.37		0.31		0.31
1790	1781	9	1816	26	2.35	2.41	0.06	35	0.257	2.37	0.32	0.36	0.04	0.33
1820	1816	4	1836	16	2.41	2.37	0.04	20	0.200	2.40	0.36	0.34	0.02	0.36
1850	1836	14	1852	2	2.37	2.30	0.07	16	0.125	2.31	0.34	0.31	0.03	0.31
1880	1876	4	1897	17	2.34	2.34	0	21	0.190	2.34	0.38	0.37	0.01	0.38
1910	1897	13	1929	19	2.34	2.32	0.02	32	0.406	2.33	0.37	0.35	0.02	0.36
1940	1929	11	1958	18	2.32	2.34	0.02	29	0.379	2.33	0.35	0.30	0.05	0.33
1970	1958	12	1975	5	2.34	2.42	0.08	17	0.294	2.40	0.30	0.36	0.06	0.34
2000	2000	0			2.41					2.41	0.35			0.35
2030	2016	14	2032	2	2.34	2.40	0.06	16	0.125	2.39	0.31	0.32	0.01	0.32
2060	2053	7	2075	15	2.42	2.37	0.05	22	0.318	2.40	0.32	0.33	0.01	0.32
2090	2075	15	2105	15	2.37	2.37	0	30	0.500	2.37	0.33	0.32	0.01	0.33
2120	2114	6	2163	43	2.39	2.39	0	49	0.122	2.39	0.37	0.29	0.08	0.36
2150	2114	36	2163	13	2.39	2.39	0	49	0.265	2.39	0.37	0.29	0.08	0.31
2180	2163	17	2184	4	2.39	2.39	0	21	0.190	2.39	0.29	0.31	0.02	0.31
2210	2205	5	2223	13	2.35	2.36	0.01	18	0.278	2.35	0.30	0.30	0	0.30
2240	2226	14	2256	16	2.39	2.37	0.02	30	0.467	2.38	0.31	0.33	0.02	0.32
2270	2256	14	2275	5	2.37	2.38	0.01	19	0.263	2.38	0.33	0.32	0.01	0.32
2300	2298	2	2349	49	2.38	2.38	0	51	0.039	2.38	0.32	0.31	0.01	0.32
2330	2298	32	2349	19	2.38	2.38	0	51	0.373	2.38	0.32	0.31	0.01	0.31
2360	2349	11	2370	10	2.38	2.36	0.02	21	0.476	2.37	0.31	0.30	0.01	0.30
2390	2370	20	2393	3	2.36	2.42	0.06	23	0.130	2.41	0.30	0.33	0.03	0.33
2420	2413	17	2434	14	2.41	2.40	0.01	31	0.452	2.40	0.33	0.33	0	0.33
2450	2434	16	2454	4	2.40	2.43	0.03	20	0.200	2.42	0.33	0.34	0.01	0.34
2480	2473	7	2494	14	2.46	2.43	0.03	21	0.333	2.45	0.35	0.34	0.01	0.35
2510	2494	6	2523	13	2.43	2.48	0.05	19	0.316	2.45	0.34	0.33	0.01	0.34
2540	2538	2	2567	27	2.42	2.44	0.02	29	0.069	2.42	0.29	0.30	0.01	0.29
2570	2567	3			2.44			3	1	2.44	0.30			0.30
2600	2600	0			2.51					2.51	0.31			0.31
2630	2629	1	2648	18	2.50	2.45	0.05	19	0.053	2.50	0.30	0.27	0.03	0.30
2660	2648	12	2671	11	2.45	2.48	0.03	23	0.478	2.47	0.27	0.28	0.01	0.28
2690	2683	7	2700	10	2.50	2.44	0.06	17	0.412	2.48	0.24	0.21	0.03	0.23
										2.40±0.05				0.32±0.03

Table 4 (Cont'd.)

Legend

1. Depth of closest bulk-property measurements above extrapolated depth.

2. Difference in depth between sample in Column 1 and extrapolated depth.

3. Depth of closest bulk-property measurement below extrapolated depth.

4. Difference in depth between sample in Column 3 and extrapolated depth.

5,6. Reported grain density (g/cm^3) at depths above and below extrapolated depth, respectively.

7. Difference between grain densities in Columns 5 and 6.

8. Total distance (feet) between analyzed samples (Column 2 + Column 4).

9. Smallest value of Columns 2 and 4, divided by value in Column 8.

10. Calculated grain density (g/cm^3) at extrapolated depth.

11.12. Reported porosities at depth given in Columns 1 and 3, respectively.

13. Difference between Columns 11 and 12.

14. Calculated porosity at extrapolated depth.

Table 5
Cumulative Frequencies of Independent Parameters,
Functional Tuffaceous Beds in USW/G-1

A. Grain Density (n = 32)

ρ_{gi} (g/cm^3)	n_i	n_i/n	$\frac{n_1+\ldots n_i}{n}$
2.31	1	0.0313	0.0313
2.32	0	0	0.0313
2.33	0	0	0.0313
2.34	0	0	0.0313
2.35	0	0	0.0313
2.36	1	0.0313	0.0626
2.37	2	0.0625	0.1251
2.38	3	0.0938	0.2189
2.39	2	0.0625	0.2814
2.40	3	0.0938	0.3752
2.41	3	0.0938	0.4690
2.42	1	0.0313	0.5003
2.43	2	0.0625	0.5628
2.44	2	0.0625	0.6253
2.45	0	0	0.6253
2.46	2	0.0625	0.6878
2.47	0	0	0.6878
2.48	2	0.0625	0.7503
2.49	3	0.0938	0.8441
2.50	1	0.0313	0.8754
2.51	1	0.0313	0.9067
2.52	0	0	0.9067
2.53	1	0.0313	0.9380
2.54	0	0	0.9380
2.55	0	0	0.9380
2.56	0	0	0.9380
2.57	0	0	0.9380
2.58	0	0	0.9380
2.59	1	0.0313	0.9693
2.60	0	0	0.9693
2.61	0	0	0.9693
2.62	0	0	0.9693
2.63	0	0	0.9693
2.64	1	0.0313	1.0

B. Porosity (n = 32)

0.27	2	0.0625	0.0625
0.28	0	0	0.0625
0.29	0	0	0.0625
0.30	1	0.0313	0.0938
0.31	0	0	0.0938
0.32	0	0	0.0938
0.33	2	0.0625	0.1563
0.34	4	0.1250	0.2813
0.35	3	0.0938	0.3751
0.36	7	0.2188	0.5939
0.37	5	0.1563	0.7502
0.38	1	0.0313	0.7815
0.39	6	0.1875	0.9690
0.40	1	0.0313	1.0

Table 6
Cumulative Frequencies of Independent Parameters,
Functional Tuffaceous Beds in UE-25a#1

A. Grain Density (n = 36)

ρ_{gi} (g/cm^3)	n_i	n_i/n	$\frac{n_1+\ldots n_i}{n}$
2.36	5	0.139	0.139
2.37	3	0.083	0.222
2.38	5	0.139	0.361
2.39	3	0.083	0.444
2.40	3	0.083	0.527
2.41	3	0.083	0.610
2.42	3	0.083	0.693
2.43	2	0.056	0.749
2.44	4	0.111	0.860
2.45	1	0.028	0.888
2.46	1	0.028	0.916
2.47	2	0.056	0.972
2.48	0	0	0.972
2.49	0	0	0.972
2.50	0	0	0.972
2.51	0	0	0.972
2.52	0	0	0.972
2.53	0	0	0.972
2.54	0	0	0.972
2.55	0	0	0.972
2.56	0	0	0.972
2.57	0	0	0.972
2.58	0	0	0.972
2.59	0	0	0.972
2.60	0	0	0.972
2.61	0	0	0.972
2.62	0	0	0.972
2.63	1	0.028	1.0

B. Porosity (n = 36)

0.22	1	0.028	0.028
0.23	1	0.028	0.056
0.24	0	0	0.056
0.25	2	0.056	0.112
0.26	3	0.083	0.195
0.27	1	0.028	0.223
0.28	1	0.028	0.251
0.29	2	0.056	0.307
0.30	2	0.056	0.363
0.31	5	0.139	0.502
0.32	3	0.083	0.585
0.33	5	0.139	0.724
0.34	5	0.139	0.863
0.35	2	0.056	0.919
0.36	1	0.028	0.947
0.37	0	0	0.947
0.38	0	0	0.947
0.39	1	0.028	0.975
0.40	1	0.028	1.0

Table 7

Cumulative Frequencies of Independent Parameters,
Functional Tuffaceous Beds in USW G-2

A. Grain Density (n = 32)

ρ_{gi} (g/cm^3)	n_i	n_i/n	$\frac{n_1+\ldots n_i}{n}$
2.31	1	0.0313	0.0313
2.32	0	0	0.0313
2.33	2	0.0625	0.0938
2.34	1	0.0313	0.1251
2.35	1	0.0313	0.1564
2.36	0	0.	0.1564
2.37	4	0.1250	0.2814
2.38	4	0.1250	0.4064
2.39	4	0.1250	0.5314
2.40	4	0.1250	0.6564
2.41	2	0.0625	0.7189
2.42	2	0.0625	0.7814
2.43	0	0	0.7814
2.44	1	0.0313	0.8127
2.45	2	0.0625	0.8752
2.46	0	0	0.8752
2.47	1	0.0313	0.9065
2.48	1	0.0313	0.9378
2.49	0	0	0.9378
2.50	1	0.0313	0.9591
2.51	1	0.0313	1.0

B. Porosity (n = 32)

0.23	1	0.0313	0.0313
0.24	0	0	0.0313
0.25	0	0	0.0313
0.26	0	0	0.0313
0.27	0	0	0.0313
0.28	1	0.0313	0.0626
0.29	1	0.0313	0.0939
0.30	4	0.1250	0.2189
0.31	6	0.1875	0.4064
0.32	5	0.1563	0.5627
0.33	5	0.1563	0.7190
0.34	3	0.0938	0.8128
0.35	2	0.0625	0.8753
0.36	3	0.0938	0.9691
0.37	0	0	0.9691
0.38	1	0.0313	1.0

thus reflect one-way projections of data or, in some cases, coincidence of extrapolated depths and depths at which bulk properties were measured. Parenthetical values in Columns 1 and 3 indicate the number of samples analyzed at a specified depth. Tables 5-7 are simply listings of the ranges and cumulative frequencies of data contained in Columns 10 and 14 of Tables 2-4, respectively.

Average calculated grain densities and porosities, listed at the bottom of Columns 10 and 14 in Tables 2-4, agree quite well with average measured values listed in Table 1. The largest difference is 0.04 g/cm^3 between measured and calculated average grain densities in UE-25a#1. Measured and calculated grain densities in USW G-1 and USW G-2 agree to within 0.01 g/cm^3. Average porosities agree to within ±0.01 in all holes.

Cumulative frequency distributions for grain densities and porosities within the functional Tuffaceous Beds based on data contained in Tables 5-7, are shown in Figures 3 and 4, respectively. As shown in Figure 3, calculated grain densities in the functional Tuffaceous Beds range from 2.31 to 2.62 g/cm^3. Lower values correspond to more completely zeolitized material. Higher grain densities, especially those >2.5 g/cm^3, are generally from within the basal bedded/reworked zone in the Tuffaceous Beds of Calico Hills. Note that no abnormally high grain densities are reported from the functional Tuffaceous Beds in USW G-2 where the basal reworked portion of the Tuffaceous Beds of Calico Hills is faulted out.

Most mineralogical analyses of materials from the functional Tuffaceous Beds indicate pervasive zeolitization, with total clinoptilolite and mordenite contents of 30% to 80%, the remainder of the mineralogy being largely feldspar and subordinate quartz.[3,7,8] If it is assumed that the feldspar/quartz ratio is 2:1 independent of zeolite content, calculated grain densities range from 2.47 g/cm^3 at 30% zeolitization to 2.25 g/cm^3 at 80% alteration. These values were calculated by assuming a grain density of 2.16 g/cm^3 for clinoptilolite,[9] and 2.65 and 2.58 g/cm^3 for quartz and feldspar, respectively. The grain density of mordenite, 2.13 g/cm^3, does not allow discrimination of zeolite species by means of bulk-property measurement.

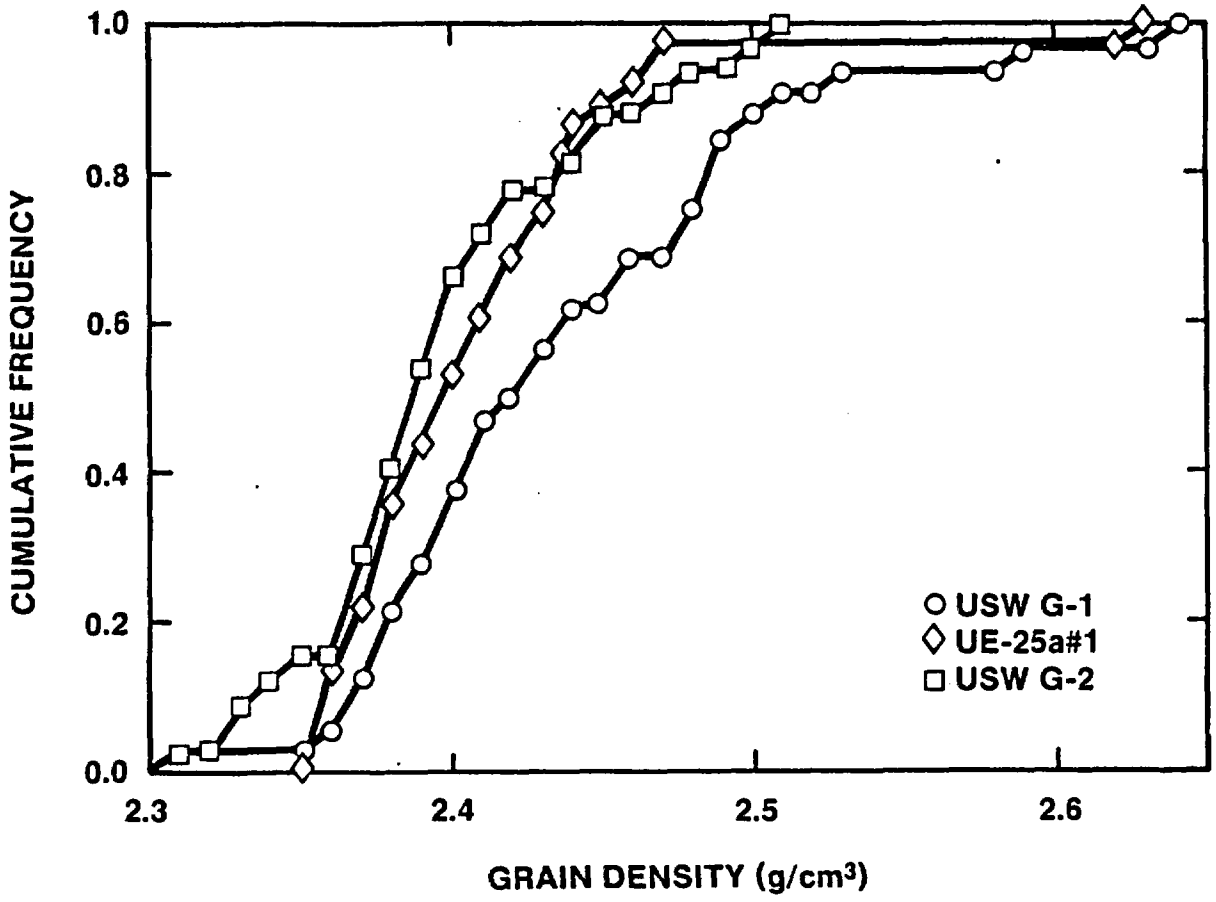

Figure 3. Cumulative Frequency Diagram of Grain Density

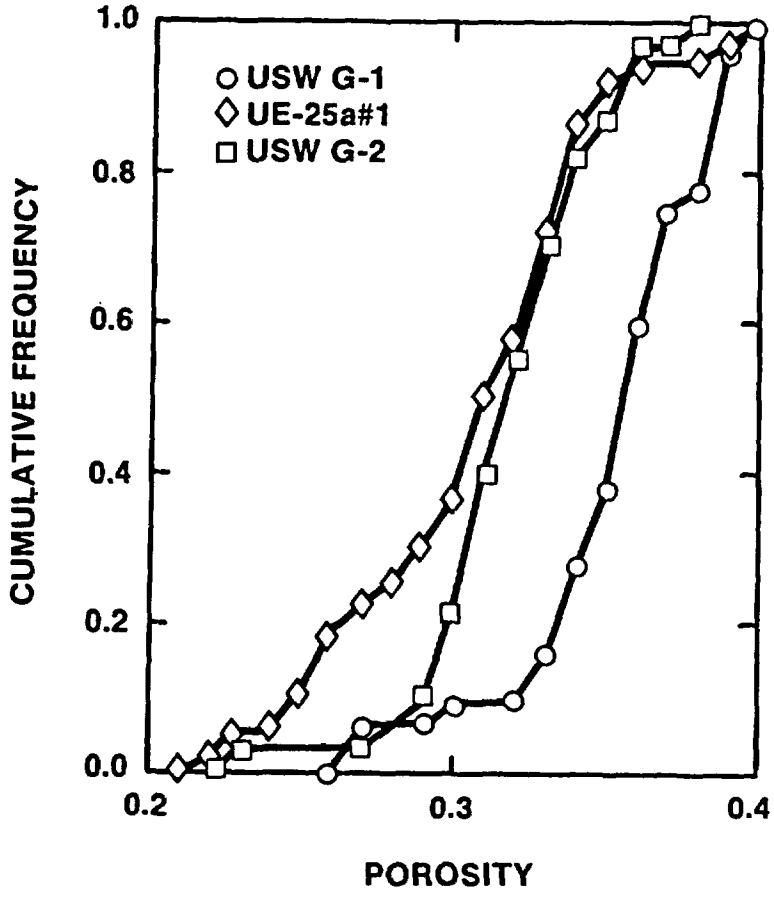

Figure 4. Cumulative Frequency Diagram of Porosity

The measured average grain densities within the functional Tuffaceous Beds, which range from 2.37 to 2.43 g/cm^3, are thus quite consistent with mineralogical analyses. These densities indicate an average zeolite content in the unit as a whole of 40% to 50%. Samples with reported grain densitites of $\geq$2.50 g/cm^3 should contain <20% zeolite.

The cumulative frequency distributions of porosity within the functional Tuffaceous Beds show little variation between holes (Figure 4). Note that the total range in calculated porosities of from 0.21 to 0.40 in the functional Tuffaceous Beds in USW G-1, UE-25a#1, and USW G-2, does not greatly exceed the estimated total range in an individual measurement (0.12). In fact, 90% or more of the frequency distribution for USW G-1 and USW G-2 is within a porosity range of $\leq$0.12; the functional Tuffaceous Beds in UE-25a#1 appear slightly more variable. These results raise the possibility that the major part of the Tuffaceous Beds in these three holes have statistically homogeneous bulk properties, even for purposes of sensitivity analyses.

THERMAL CONDUCTIVITY

The variability in thermal conductivity of a functional unit is estimated in a three-step process. First, the boundaries of the unit and the distributions of porosity and grain density with the unit must be determined. Second, the distribution of zero-porosity or matrix conductivity within the unit must be determined as a function of mineralogy and/or grain density, if possible. Finally, estimated in situ conductivities (not including possible effects of fracturing), can be calculated from estimated matrix conductivities and reported porosity distribution.

It is concluded that, except possibly for the thick bedded/reworked zone at the base of the Tuffaceous Beds of Calico Hills, the matrix of the functional Tuffaceous Beds is homogeneous relative to uncertainties in bulk-property measurements, mineralogical analyses, and measurements of thermal conductivity. Grain densities and porosities are believed to be precise to ±0.06 g/cm^3 and ±0.06, respectively.[10] Mineralogical

analyses, which were carried out by semiquantitative bulk x-ray techniques,[3] are of varying reliability, depending on the minerals involved. Thermal conductivity measurements are precise to within ±10 percent.[10] However, a presently ongoing detailed examination of thermal conductivity and mineralogy within the functional Tuffaceous Beds may yet reveal consistently coupled variations.

As of March 15, 1982, thermal conductivities were measured successfully on 13 strongly zeolitized tuffs from USW G-1, UE-25a#1, and USW G-2. Table 8 summarizes these measurements. Five of the measurements were made on material from the functional Tuffaceous Beds as defined here. The zero-porosity or theoretical matrix conductivity of these five samples, calculated by the geometric-means approach,[10] is 1.86 ±0.18 W/m•K. The calculated matrix conductivity of the other eight zeolitized samples is 2.00 ±0.18 W/m•K. These values do not differ significantly. The zero-porosity or matrix conductivity of heavily zeolitized tuffs therefore appears effectively constant near 1.95 W/m•K regardless of lateral or vertical position and detailed mineralogy.

This conclusion is supported here in two ways. First, as shown in Figure 5, no apparent correlation exists between zero-porosity conductivity and reported grain density (extent of zeolitization) over the range of reported grain densities between 2.3 and 2.5 g/cm^3. Second, as shown in Figure 6 and Table 9, the cumulative frequency distribution of calculated theoretical zero-porosity conductivities is nearly linear over the entire range of reported values, between 1.6 and 2.2 W/m•K, corresponding to a random distribution. Unfortunately, the thermal conductivities of pure clinoptilolite and mordenite (the dominant zeolites within the Tuffaceous Beds) remain unknown. Until data for these thermal conductivities are acquired, it is impossible to calculate a theoretical matrix conductivity for these tuffs. The approach that must be taken is therefore, strictly empirical.

Table 8

Summary of Thermal-Conductivity Measurements of Heavily Zeolitized Tuffs

Hole and Depth (ft)	K_o (W/m•K[a])	Grain Density (g/cm^3)	Porosity (Calc.)	$K^{S=1.0}_{meas}$ (W/m"K)	$K^{S=0}_{meas}$[b] (W/m"K
G1-1395	1.89	2.44	0.35	1.27	0.97
G1-1503	2.08	2.48	0.38	1.31	1.00
G1-1706	1.62	2.33	0.33	1.21	--
G1-2010	1.71	2.40	0.28	1.36	0.92
G1-2070	1.83	2.41	0.29	1.41	0.94
G1-2274.4	2.09	2.36	0.34	1.40	1.09
G1-2310	2.24	2.44	0.37	1.41	1.07
G1-2311	2.19	2.41	0.36	1.42	0.99
G1-2568	1.90	2.41	0.30	1.41	1.05
G1-2569	2.01	2.44	0.32	1.41	1.17
G1-2701	2.02	2.42	0.31	1.43	1.11
G2-1721	1.96	2.37	0.30	1.38	1.07
A1-1569	1.77	2.46	0.33	1.27	0.76

K_o for 13 zeolitized tuffs = 1.95±0.18 W/m•K.

Porosity of samples analyzed = 0.33±0.03.

Saturated conductivity = 1.36±0.07 W/m•K.

Dehydrated conductivity = 1.01±0.11 W/m•K.

a: $K_o = \left(\frac{K^{S=1.0}_{meas}}{K^{\phi}_{water}} \right)^{\frac{1}{1-\phi}}$, where K_{water} is taken as 0.61 W/m•K and

ϕ is total calculated porosity.

b: Measured at temperature of ≥200°C.

S: Saturation (volume fraction).

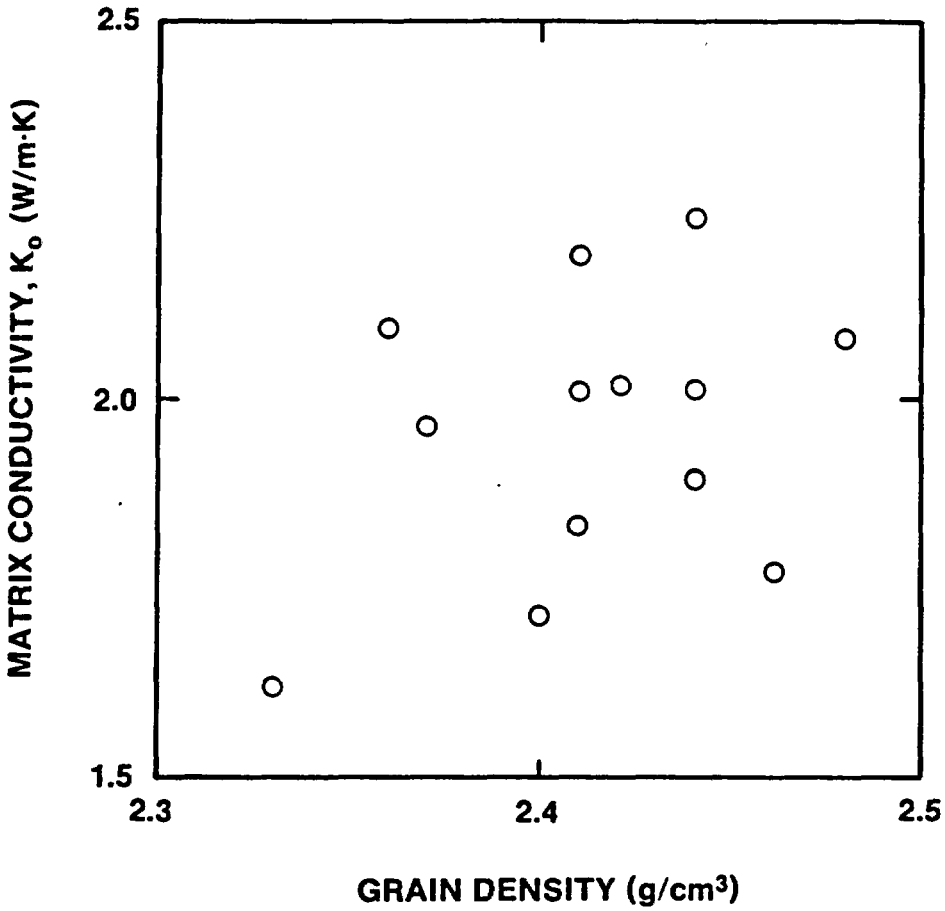

Figure 5. Grain Density Versus Matrix Thermal Conductivity

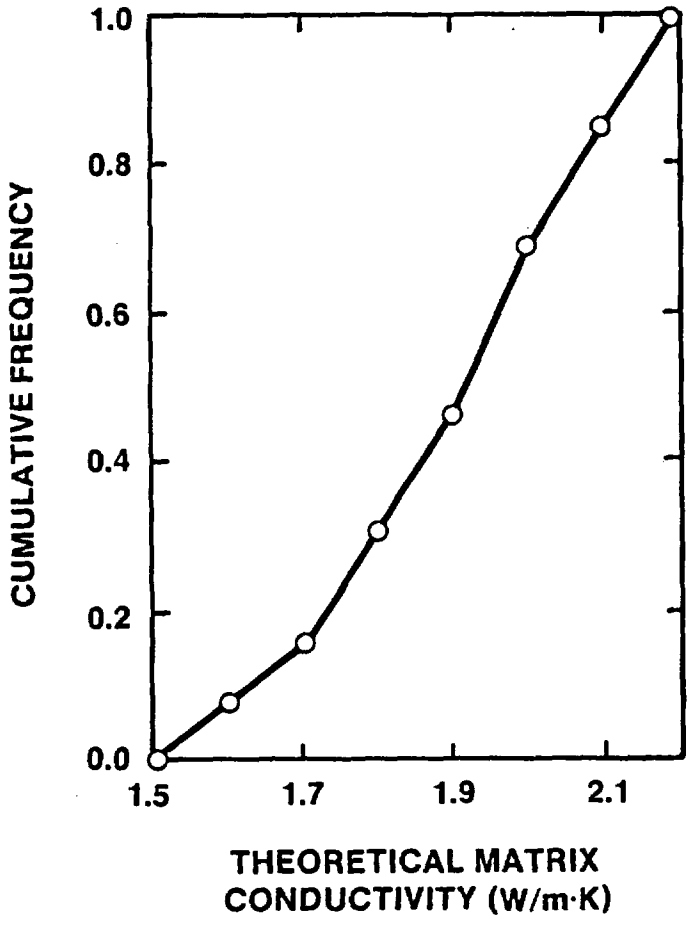

Figure 6. Cumulative Frequency Diagram of Matrix Thermal Conductivity

Table 9

Cumulative Frequency of Theoretical Matrix Conductivity of Strongly Zeolitized Tuffs

Ko_i (W/m•K)	n_i	n_i/n	$\frac{n_1+\ldots n_i}{n}$
1.6	1	0.077	0.077
1.7	1	0.077	0.154
1.8	2	0.154	0.308
1.9	2	0.154	0.462
2.0	3	0.231	0.693
2.1	2	0.154	0.847
2.2	2	0.154	1.0

It remains to calculate the average saturated thermal conductivity for the functional Tuffaceous Beds in the three exploratory holes. The unitwide average grain density and porosity are 2.40 g/cm^3 and 0.32, respectively (Table 1). Average grain densities range from 2.37 g/cm^3 in UE-25a#1 to 2.43 g/cm^3 in USW G-1; average porosities range from 0.30 in UE-25a#1 to 0.35 in USW G-1. Assuming a zero-porosity thermal conductivity of 1.95 W/m•K, this leads to a calculated average saturated conductivity for the functional Tuffaceous Beds as a whole of 1.34 W/m•K. This compares to an average measured conductivity for all zeolitized tuff (13 samples) of 1.36 ±0.07 W/m•K. Estimated unitwide conductivities range from 1.29 W/m•K in USW G-1 to 1.37 W/m•K in UE-25a#1. If the cumulative porosity data in Figure 4 are correct, 80% of the total thickness of the functional Tuffaceous Beds in USW G-1, UE-25a#1, and USW G-2 should have a saturated conductivity of between 1.24 and 1.46 W/m•K, based on the average matrix conductivity of 1.95 W/m•K. If a conservative matrix conductivity of 1.75 W/m•K is assumed, this range becomes 1.16 to 1.34 W/m•K.

The porosity distributions in Figure 4 include both the bedded/reworked zone at the base of the Tuffaceous Beds of Calico Hills and the underlying zeolitized portion of the Prow Pass Member. On the other hand, if only the upper part of the functional Tuffaceous Beds is considered (Table 1), average saturated conductivities would range from 1.28 to 1.36 W/m•K at matrix conductivity of 1.95 W/m•K, and 1.19 to 1.26 W/K at 1.75 W/m•K matrix conductivity. The average saturated conductivity of the bulk of the functional Tuffaceous Beds is thus 1.3 W/m•K.

Measured dehydrated conductivities of these tuffs (Table 8) average 1.0 W/m•K. However, most of the measurements in Table 8 were made at confining pressures of 10 MPa and fluid pressures of 1.5 MPa[10] to simulate in situ saturated conditions. As a result, the measurements on dehydrated samples were made at temperatures of ≥200°C. Recent data, to be reported in detail in a separate report, suggest an increase of about 15% in the dehydrated conductivity of zeolitic tuffs between ambient temperature and 200°C. Based on these results, an average dehydrated conductivity of 0.9 W/m•K is considered conservative at or near 100°C for the tuffs analyzed in Table 8. This conductivity was recommended for modeling purposes.

THERMAL EXPANSION

Primary factors that control temperatures resulting from waste emplacement are thermal loading and thermal conductivity. A major factor controlling thermally induced strains near an underground waste repository is the behavior of thermal expansion. The nature of the thermally induced strain depends on the general pattern of such behavior. If expansion coefficients on heating are greater than zero, stresses will be largely compressive and the necessary coupling of thermal and mechanical properties minor. However, if contraction occurs on heating, the interactions are potentially more complex. If the thermally induced stress caused by contraction exceeds the compressive stress resulting from initial in situ conditions, tensile fracturing can occur in the heated environment either because preexisting fractures open or new ones form.

The formation of open fractures, especially if they are air-filled, could have some impacts. First, the mechanical integrity of the rockmass might be degraded. Secondly, variations in joint aperture might require extensive coupling of mechanical, thermal, and fluid-transport properties in modeling.

Preliminary measurements of unconfined thermal expansion, and a review of the literature both indicate that thermal expansion of rocks should be effectively independent of porosity (except for planar microcracks). This behavior is expected if (1) pore collapse does not occur at high pressures,[11] and (2) fluids released during dehydration escape quickly relative to increases in temperature, thus avoiding significant fluid overpressurization.

The thermal expansion behavior of zeolitized or altered tuffs is potentially quite complex because of the presence of one or more hydrated phases. These phases are discussed individually in the following paragraphs.

The major component of most fresh silicic tuff is silicic glass. This glass often contains ~0.5 wt % "magmatic" water entrapped at high temperatures and not given off on moderate heating ($\leq$300°C). After emplacement, initially "anhydrous" glasses are often hydrated as a result of interaction with

deuteric fluids (postmagmatic but still hydrothermal) or with groundwater, and may contain ≥7% water.[12,13] The detailed structural consequences of low-temperature glass hydration are unclear, except that hydration involves a decrease in the density and refractive index of the glass, and at least some expansion.[12,13] No detailed information is available for volumetric changes resulting from hydration of silicic glass or for local variations in the extent of hydration within the tuffs at Yucca Mountain. Fortunately, glass is generally absent in strongly zeolitized tuffs from Yucca Mountain.[3,7,8] Shallower tuffs are often vitric; locally they contain strongly hydrated glasses.[8]

Downward-migrating tuff groundwaters soon become saturated with silica, largely by leaching from overlying units.[14] This can lead to precipitation of opal in the fractures and matrix of many tuffs, even above the static water level. Opal in tuffs from Yucca Mountain is reportedly a cryptocrystalline mixture of amorphous material, quartz, and cristobalite.[3] The structural details of this phase are unclear, partly because the x-ray pattern of many opals is virtually indistinguishable from that of anhydrous cristobalite. All that can be said with certainty is that opal generally contracts when dewatered, and dehydration can occur at low temperatures.

Reported opal-cristobalite contents within the functional Tuffaceous Beds are 5% to 30% in USW G-2[8] and 2% to 30% in USW G-1.[3] No general distribution pattern is evident in the analyses. Estimated opal-cristobalite abundances may be strongly affected by overlap between feldspar and opal-cristobalite x-ray peaks in samples containing appreciable feldspar.[3]

Clays are widespread in tuffs (see, for example, Refs 8 and 15). Virtually all clays encountered at Yucca Mountain, especially at depths of <~3500 feet, are "expandable" and, by analogy, "contractable."[15] This means that their structural state depends on both temperature and relative humidity.

The effect of expandable clays on thermal expansion could be drastic. The report by Bish[15] indicates that most of the expandable clays in core from USW G-1 are Na-saturated. This type of smectite or montmorillonite (when

pure) changes basal spacing from 17 A at full saturation to near 11 A when exposed to low-humidity air at ambient temperature. Heating reduces basal spacing to near 10 A. The in situ basal spacing of such clays remains largely unknown. A rock consisting totally of such clay theoretically could contract by as much as 35 linear percent relative to its initial length as a result of ambient temperature dehydration. If heated, contraction could reach a theoretical maximum of ~40%.

The clay content of heavily zeolitized tuffs appears generally to increase with depth at Yucca Mountain. Total clay contents in the functional Tuffaceous Beds as defined here (except possibly for the lower portions of the Topopah Spring Member) are generally <5%.[3,8] By contrast, zeolitized portions of the Tram Member generally have clay contents of 10% to 20%.[8,15]

Lateral variability in clay distribution appears to increase with increasing depth. Both vertical and lateral extrapolation of clay mineralogy in zeolitized tuffs is risky, since no reliable model exists describing the genesis of the clays. Structural effects, especially faulting, may lead to local variations in clay alteration.

The major secondary phases present in the functional Tuffaceous Beds are zeolites. Some of these zeolites may result from in situ chemical alteration of silicic glass; some may have precipitated from groundwater in pores. Note that the zeolites so characteristic of the functional Tuffaceous Beds are entirely secondary; their distribution depends on hydrologic and perhaps thermal history. Because the details of the hydrologic and thermal history are not available, the distribution of zeolites cannot be predicted reliably.

Three main zeolites occur in the tuffs at Yucca Mountain: clinoptilolite-heulandite, mordenite, and analcime. Analcime is restricted almost entirely to deeper tuffs and is not found in the functional Tuffaceous Beds. Clinoptilolite and heulandite form an apparently continuous compositional series; heulandite is Ca-, Al-rich and clinoptilolite is Na-, K-, Si-rich. Because of the great difference in the thermal stability of the

two end members, the solid solution is of some importance. Mordenite is quite similar in composition to Na-clinoptilolite, but is apparently stable to higher temperatures[8].

In short-term heating tests, heulandite becomes amorphous, as indicated by x-rays, at temperatures as low as 250°C; clinoptilolite is stable to 700°C.[16] The thermal stability of intermediate species is largely unknown. Mineralogical analyses of samples from USW G-2[8] indicate a consistent shift in composition of clinoptilolite-heulandite zeolites with depth. The uppermost zeolites contain ~70% Ca/(Ca + K + Na), and would properly be classed as heulandites. In the Tuffaceous Beds of Calico Hills, vug- and pumice-filling zeolites contain ~40% Ca/(Ca + K + Na). Clinoptilolite in the Prow Pass Member is almost Ca-free. At greater depths, mordenite and analcime predominate over clinoptilolite, and Na/(Ca + K + Na) increases markedly.

Several factors thus limit developing a theoretical understanding of the thermal-expansion behavior of zeolitized tuffs and a lateral predictive capability:

- The dominant hydrated minerals in zeolitized tuffs, namely zeolites, opal-cristobalite, and clays, are all secondary in origin. Distribution of these secondary phases depends on external variables. Without knowledge of these variables, distribution cannot be predicted reliably at present.

- The secondary phases of interest show broad ranges in composition, structural state, and thermal stability. Further, data on the thermal stability of many of the pure phases do not exist.

- It is not clear what fractions of the hydrous phases present actually serve as effective load-bearing structural members within the tuff matrix. If any phase is not load-bearing, its contraction at dehydration would have no effect on overall rock behavior but would merely increase porosity.

Therefore, the approach taken here is to examine the results of thermal-expansion measurements on zeolitized tuffs to date to determine their reliability or consistency for engineering purposes. Little effort goes toward theoretical considerations.

Three basic temperature domains exist across which the thermal expansion of zeolitic tuffs must be understood: (1) predehydration; (2) transdehydration, and (3) postdehydration. These domains are discussed at length below.

Predehydration Expansion: For waste emplacement below the water table, dehydration (except along the walls of emplacement drifts) would occur only at temperatures $\geq$100°C. The temperatures at which dehydration occurs would be controlled by both the natural and thermally induced hydrostatic heads. The temperature range over which predehydration expansion would occur may depend on local heating rates and fluid pressures, but not the predehydration expansion coefficient itself unless fluid overpressurization occurred.

Reliable measurements of predehydration expansion can be made only in confined tests, since unconfined samples begin to dehydrate as soon as they are placed on the dilatometer. As of March 15, 1982, seven confined expansion measurements (summarized in Table 10) were made on heavily zeolitized samples. Of the seven samples, five are from the Tuffaceous Beds of Calico Hills and two are from tuffs at greater depths. The measurements were made at Terra Tek, Inc. in Salt Lake City, at a confining pressure of 10 MPa and a fluid pressure of 0.3 MPa. At this fluid pressure, the boiling point of water is 133°C. Sample cylinders 10.3 cm long and 5.1 cm in diameter were heated at a rate of 1-2°C/min before dehydration. Estimated precision of the test apparatus is $\pm 1.5 \times 10^{-6}\ K^{-1}$. The predehydration coefficient of the five samples from the Tuffaceous Beds of Calico Hills averages $7.4 \pm 3.9 \times 10^{-6}\ K^{-1}$. If all samples are included, the average value is $6.7 \pm 3.7 \times 10^{-6}\ K^{-1}$. For modeling purposes, it should be assumed initially that all heavily zeolitized tuffs expand at an average rate near $7.0 \times 10^{-6}\ K^{-1}$ to the onset of dehydration. The measured coefficients range from 2.8 to $13.2 \times 10^{-6}\ K^{-1}$.

Table 10

Linear Thermal Expansion
of Zeolitized Tuffs

Sample	Unit	Linear Expansion Coefficient (10^{-6} K^{-1}) to Near 125°C
G1-1450	Tht	13.2
G1-1619	Tht	8.5
G1-1762	Tht	3.4
G1-1772	Tht	8.2
G1-2286	Tcb	2.8
G1-2562	Tcb	6.8
G2-2498	Tht	3.9
Avg. of 7 samples		6.7 ±3.7

Measurements made at confining pressure of 10 MPa and nominal fluid pressure of 0.3 MPa, at a heating rate of 1° to 2°C/min.

Tht: Tuffaceous Beds of Calico Hills.
Tcb: Bullfrog Member

Transdehydration Expansion: Behavior of zeolitized tuffs during dehydration is quite variable. Available data appear to categorize this behavior into three types: (1) nonwelded, zeolitized ashflow tuffs, (2) zeolitized, partially welded and nonwelded zones with relatively high combined quartz and feldspar contents, and (3) bedded/reworked portions of the unit. Types 1 and 2 display relatively strong cross-coupling of expansion behavior and mineralogy. Data for Type 3 provide an inadequate statistical base for detailed characterization of expansion behavior. A general discussion of transdehydration thermal expansion behavior is presented in this section.

Mineralogical analyses (Refs 3, 8, and unpublished analysis by S. Levy and D. Vaniman of Los Alamos National Laboratory) indicate that the ashflow portions of the functional Tuffaceous Beds, besides being heavily zeolitized, generally have low quartz and feldspar contents. Given that the linear expansion coefficient of polycrystalline quartz increases from 13×10^{-6} K^{-1} at 100°C to 18×10^{-6} K^{-1} at 300°C, the presence or absence of quartz can have a qualitative impact. The reported linear expansion of orthoclase (alkali feldspar similar to that found in devitrified tuffs) varies from 3 to 6×10^{-6} K^{-1} over the same temperature interval.[17]

The transdehydration thermal expansion of most of the functional Tuffaceous Beds appears dominated by a combination of strong zeolitization (intermediate clinoptilolite and/or mordenite) and low quartz and feldspar contents. As of March 15, 1982, unconfined expansion was measured on samples from 11 different depths within the ashflow portions of the unit: six in UE-25a#1, four in USW G-1, and one in USW G-2.

The maximum contraction resulting from dehydration and the general pattern of expansion behavior vary from hole to hole and within each hole (Table 11). In the case of samples of nonwelded, zeolitized ashflows from USW G-1 (1 in Table 11), maximum relative contraction averages 0.003 ±0.0008 in./in., at a temperature ~250°C. The temperature of maximum contraction is only approximate for these tuffs, since these samples contract fairly rapidly to temperatures near 150°C, and then more slowly to temperatures ~300°C. Above this temperature, further contraction begins because of the removal of true framework-structural water from the zeolites. This type of behavior, thought

Table 11

Summary of Contractions Relative to Initial Length During Unconfined Linear Expansion Measurements on Heavily Zeolitized Tuffs

	Hole and Depth (ft)	Maximum Contraction (in./in.) Relative to Initial Length	Temperature of Maximum Relative Contraction (°C)
1.	G1-1423.3	0.0035	313
	-1451.1	0.003	290
		0.002	180
	-1620	0.0039	---
	-1652	0.0026	275
		Average of 5 samples: 0.003 ±0.0008	
2.	A1-1544	0.0012	158
	-1569	0.0011	150
	-1561	0.0011	150
	-1366.5	0.00175	160
	-1547.6	0.0021	175
	-1718.2	0.0015	200
	G2-2498.9	0.0012	175
		Average of 7 samples: 0.0014 ±0.0004	
3.	G1-1763	0.0008	135
	-1773.3	0.0011	140
	-1721.6	0.0010	130
	G2-2581.1	0.0005	125
		Average of 4 samples: 0.0009 ±0.0003	

to reflect almost entirely the thermal behavior of the clinoptilolite in the samples (50% to 90%), is qualitatively and quantitatively similar to the expansion behavior of strongly zeolitized tuffs from other locations.[11]

Transdehydration behavior in the ashflow portions of the functional Tuffaceous Beds in UE-25a#1 and in the lowest part of the unit in USW G-2 (2 in Table 11) begins with an average of 0.0014 in./in. net maximum relative contraction at a temperature of ~165°C. At higher temperatures these samples begin to expand, though generally not to their original length. The expansion at higher temperatures is apparently in response to a higher quartz and feldspar content in these samples relative to analogous tuffs in USW G-1.[3,8] The average combined quartz and feldspar content reported in ashflow portions of the functional Tuffaceous Beds in USW G-2 increases from 23% above 2353 ft to 55% below this depth, with a corresponding decrease in total zeolite content from 50% to 90% to <50%.[8] Similar detailed analyses are not available for UE-25a#1. In USW G-1 the average reported combined quartz and feldspar content in the ashflow portions of the Tuffaceous Beds of Calico Hills is 29% ±15%, similar to that in the upper part of the unit in USW G-2. If mineralogy is indeed the controlling factor, the major part of the functional Tuffaceous Beds in USW G-2 (that portion from 1680 ft to approximately 2353 ft depth) should behave much like the nonwelded ashflows from the Tuffaceous Beds of Calico Hills in USW G-1, rather than as seen in UE-25a#1 and the lowest ashflow in USW G-2. The transdehydration behavior of the functional Tuffaceous Beds in UE-25a#1 and USW G-2 is similar, however, to that of zeolitized, partially welded ashflows deeper in USW G-1. Nine unconfined tests on these materials show an average net maximum contraction of 0.0013 in./in. at a temperature of ~175°C.

A third and apparently distinct group of expansion results is from materials in the bedded/reworked zones in USW G-1 and USW G-2 (3 in Table 11). Mineralogical results indicate that these samples often have a higher combined quartz and feldspar content than do most of the zeolitized ashflows. Tuffaceous sandstones are also sometimes present. The expansion behavior in bedded/reworked zones studied to date (based on only four samples) is thus not representative as a result of the mineralogical complexity of

these zones. The maximum thermal contraction of the analyzed samples from bedded/reworked zones averages 0.0009 ±0.0003 in./in. and occurs at a temperature of ~135°C. All these samples expand beyond their initial length with continued heating.

In summary, transdehydration behavior within the functional Tuffaceous Beds can apparently be divided into three types. In all cases, the behavior described below assumes that the tuffs begin to dehydrate near the boiling point of water, effectively 100°C. Transdehydration expansion coefficients are then estimated by combining net contractions measured during unconfined tests with predehydration expansion coefficients determined in confined tests.

Type 1. **Nonwelded, zeolitized ashflow tuffs,** at least material within the Tuffaceous Beds of Calico Hills with a low combined quartz and feldspar content, contract an average of 0.3% at a temperature of 300°C. Contraction is most rapid to 150°C, where it averages 0.23%. If the predehydration expansion coefficient is 6.7×10^{-6} K^{-1}, then a net contraction of 0.0023 in./in. at 150°C requires the expansion coefficient between 100° and 150°C to be -56×10^{-6} K^{-1}. Data presently available indicate that this behavior should apply to all the ashflows in the Tuffaceous Beds of Calico Hills in USW G-1, and to those above a depth of ~2353 ft in USW G-2.

Type 2. **Zeolitized, partially welded and nonwelded zones with relatively high combined quartz and feldspar contents** contract an average of 0.14% at a temperature of 165°C. Assuming that the predehydration coefficient is again 6.7×10^{-6} K^{-1}, this requires a transdehydration coefficient of -29.4×10^{-6} K^{-1}, between 100° and 165°C. Present data suggest that this behavior is appropriate for all the ashflows in the functional Tuffaceous Beds in UE-25a#1, and for the part of the unit between 2353 and 2704 ft in USW G-2.

Type 3. **Bedded/reworked portions of the unit** appear to undergo a linear contraction of 0.09% by ~135°C. Assuming the same predehydration coefficient as above, this requires a transdehydration coefficient of -40×10^{-6} K^{-1} between 100° and 135°C. Data for the

bedded/reworked zones are inadequate to provide a statistical base. Almost certainly behavorial types 1 and 2 will occur locally within bedded/reworked zones.

Postdehydration Expansion: Unconfined postdehydration expansion of zeolitized tuffs also appears to be a function of mineralogy. The more quartz and feldspar a sample contains, the more it expands after dehydration. This leads to identifying three postdehydration behaviors within the functional Tuffaceous Beds:

1. In the zeolite-rich ashflow tuffs with low combined quartz and feldspar content that make up most the unit, the postdehydration expansion coefficient is $-4.5 \times 10^{-6}\ K^{-1}$ between temperatures of 150° and 300°C. Above 300°C these tuffs contract at a rate $\sim -7 \times 10^{-6}\ K^{-1}$.

2. Nonwelded and partially welded ashflows with relatively high combined quartz and feldspar contents show an average expansion coefficient of $+4.4 \pm 1.9 \times 10^{-6}\ K^{-1}$ between 165° and 300°C. Above this temperature, since they still contain appreciable zeolites, they either cease expansion or they contract slightly. The very high temperature coefficient (above about 300°C) averages $-1.5 \pm 2 \times 10^{-6}\ °K^{-1}$.

3. Samples from the basal bedded/reworked portion of the Tuffaceous Beds of Calico Hills expand at an average rate of $7.8 \pm 0.9 \times 10^{-6}\ K^{-1}$ between the temperature of maximum contraction 135°C, and the peak measurement temperature, 400°C. The postdehydration expansion of three of the four samples is effectively linear; that of the fourth shows a slight decrease in the rate of expansion at ~ 350°C, presumably as a result of the high-temperature breakdown of zeolites.

Table 12 summarizes thermal expansion behavior within the functional Tuffaceous Beds. The behavior is shown schematically in Figure 7. Values listed are a mix of confined, unconfined, and composite expansion coefficients, all of them measured or calculated for heating. Fewer data on cooling are presently available, but they appear to be bounded by two limits.

Table 12

Estimated Linear Thermal Expansion of Rock Types Within the Functional Tuffaceous Beds in USW G-1, UE-25a#1, and USW G-2

Subunit or Rock Type	Expansion Coefficient (10^{-6} K^{-1})	Temperature Range (°C)
Entire Unit	6.7	ambient to 100 or ambient to T_{boil}
(Quartz + Feldspar)-poor nonwelded ashflows	56	100-150 or T_{boil}-(T_{boil}+50)
	- 4.5	150-300 or (T_{boil}+50)-(T_{boil}+200)
(Quartz + Feldspar)-rich nonwelded and partially welded ashflows	29.4	100-165 or T_{boil}-(T_{boil}+65)
	+ 4.4	165-300 or (T_{boil}+65)-(T_{boil}+200)
Bedded/Reworked Tuffs	-40	100-135 or T_{boil}-(T_{boil}+35)
	+ 7.8	135-400 or (T_{boil}+35)-(T_{boil}+300)

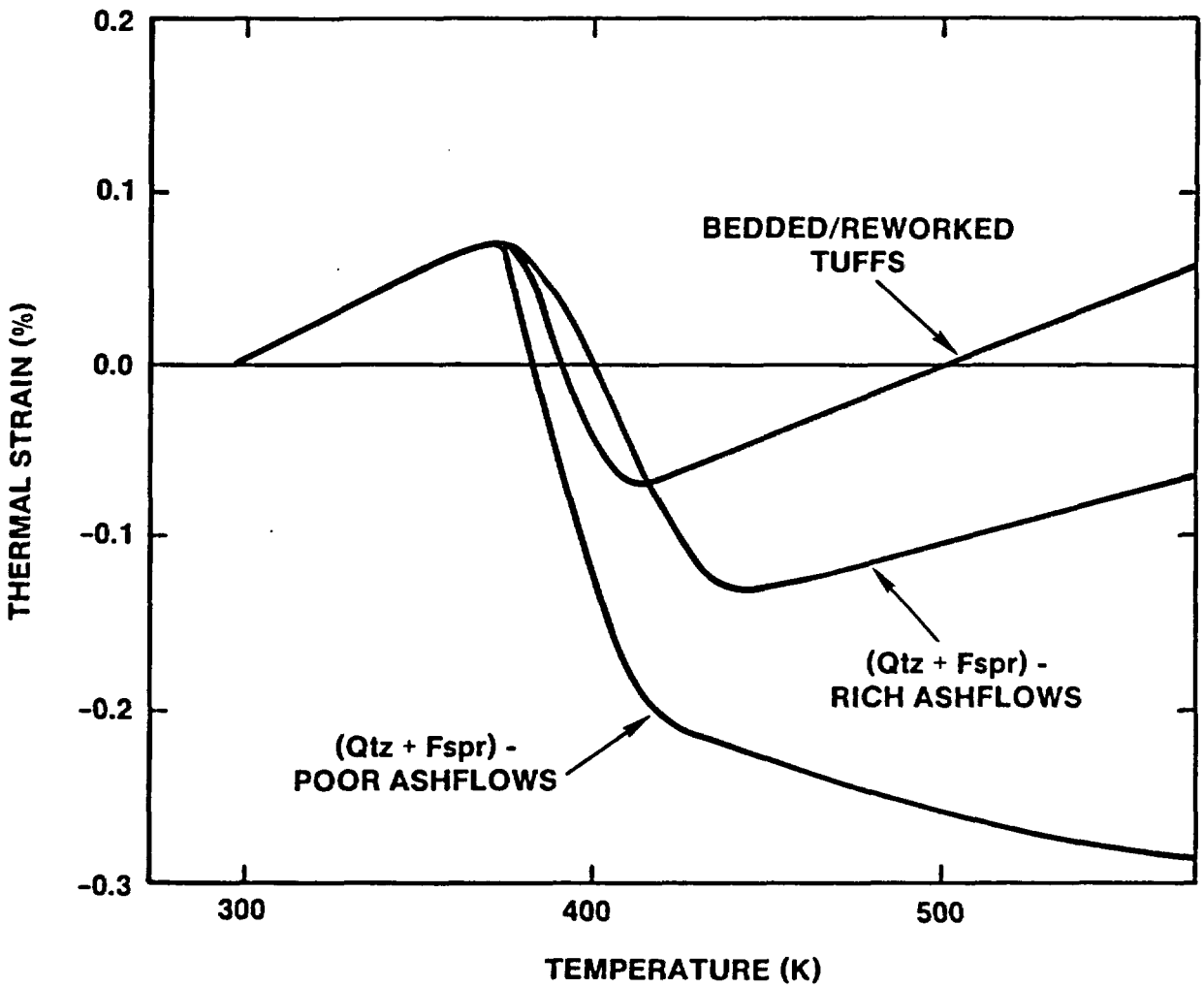

Figure 7. Schematic Representation of Thermal Expansion Behavior in the Functional Tuffaceous Beds

If it is assumed that the tuffs are dehydrated during heating but do not rehydrate on cooling, they contract on cooling at a rate near the magnitude of the postdehydration coefficient on heating. Ashflows with low combined quartz and feldspar contents contract in the postdehydration regime during both heating and cooling. The assumption of no rehydration results in net shrinkage of all rock types within the Tuffaceous Beds on return to ambient temperature, consistent with both confined and unconfined experimental results. Alternatively, if the assumption of full rehydration on cooling is made, and if the possibility of volumetric creep or pore collapse is ignored, the expansion behavior on cooling would simply be the opposite of that on heating in all temperature intervals, and the net volume change on return to ambient temperature would be zero.

Finally, two temperature ranges are specified for all expansion coefficients in Table 12. The first assumes that the effective beginning of dehydration is at 100°C. That is, neither fluid overpressurization nor dehydration occurs at temperatures below the boiling point of water. The second temperature range assumes that dehydration occurs in response to a locally elevated head potential and boiling point, and ignores the possibility of dehydration at lower temperatures.

Unconfined expansion measurements on small samples, and tunneling experience in zeolitized, nonwelded tuffs at the Nevada Test Site indicate that these tuffs can be at least partially dehydrated at temperatures well below the boiling point of water. Such dehydration leads to contraction. Although this low-temperature contraction is not included in the expansion coefficients recommended in this report for thermal/mechanical modeling, the recommended coefficients are expected to predict more contraction that actually occurs in situ.

SUMMARY

The functional Tuffaceous Beds are defined here on the basis of lithologic logs, mineralogical analyses, downhole density logs, and bulk-property measurements. They range in total thickness from 143 m in USW G-1 to 312 m in USW G-2. If the basal bedded/reworked portions of the Tuffaceous Beds of

Calico Hills and the Topopah Spring Member are excluded, a zone of heavily zeolitized, largely ashflow tuffs between 95 and 289 m thick is present within the functional Tuffaceous Beds in the triangular area defined by USW G-1, UE-25a#1, and USW G-2 (Figure 1 and Table 1).

Zeolitization is generally pervasive within the functional Tuffaceous Beds, with most analyses indicating zeolite contents of 30% to 80%. Corresponding grain densities are 2.25 to 2.47 g/cm^3. Based on extrapolation of measured results, vertical distributions of grain density and porosity suggest that the functional Tuffaceous Beds are effectively homogeneous, except for bedded/reworked zones. Unit-wide median grain densities range from only 2.38 to 2.42 g/cm^3 in the three exploratory holes considered; median porosities range from 0.31 to 0.36 (Figures 3 and 4). Grain density and porosity of 2.39 g/cm^3 and 0.33, respectively, are representative for the nonwelded ashflows within the Tuffaceous Beds of Calico Hills, which comprise the majority of the unit.

At present, the bulk and thermal properties of the many thin bedded/reworked zones within the thick ashflow sequence in the Tuffaceous Beds of Calico Hills remain largely unknown. These zones were penetrated 24 times in USW G-1, UE-25a#1, and USW G-2; they average 1.0±1.3 m in thickness. In contrast, the bedded/reworked zone at the base of the Tuffaceous Beds of Calico Hills is 14 m thick in UE-25a#1 and 20 m thick in USW G-1. The analogous zone at the base of the Topopah Spring Member is 1 m thick in UE-25a#1, 7 m thick in USW G-1, and 17 m thick in USW G-2. It is tentatively assumed here that the relatively thin bedded/reworked zones within the bulk of the Calico Hills either have material properties differing only negligibly from those of surrounding nonwelded ashflows, or their relative thickness allows them to be ignored.

As a result of inherent tuff variability and uncertainties in measurements of both bulk properties and thermal conductivity, there is no apparent trend of theoretical matrix conductivity with either mineralogy or bulk properties (Figure 5). This problem is increased by the present lack of conductivity data for pure zeolites. Nonetheless, thermal conductivity measurements on zeolitized ashflow tuffs are relatively consistent, indicating a zero-porosity

conductivity of 1.95±0.18 W/m•K. Use of this matrix conductivity indicates that the saturated conductivity in 80% of the functional Tuffaceous Beds should range between 1.2 and 1.5 W/m•K. At the average ashflow porosity of 0.33, the average saturated conductivity should be 1.3 W/m•K. Dehydrated conductivity of the average nonwelded ashflow, allowing for temperature effects between confined and unconfined tests, should be ~0.9 W/m•K. No conductivity data are presently available from bedded/reworked zones.

Internal complexity of the functional Tuffaceous Beds is apparent in thermal expansion behavior. Available confined measurements indicate a predehydration linear-expansion coefficient of $6.7 \pm 3.7 \times 10^{-6}\ K^{-1}$, with a range from 2.8 to $13.2 \times 10^{-6}\ K^{-1}$. Analyses are not yet detailed enough to define any coupling of predehydration expansion with mineralogy. Transdehydration expansion in the functional Tuffaceous Beds varies strongly, apparently because of variable quartz and feldspar content as well as variable zeolite contents, but it consistently involves contraction. Assuming dehydration begins at 100°C, a transdehydration coefficient of $-56 \times 10^{-6}\ K^{-1}$ appears appropriate for the nonwelded ashflows comprising the major part of the unit and seems to be conservative elsewhere. Transdehydration expansion coefficients average $\sim -29 \times 10^{-6}\ K^{-1}$ for partially welded zeolitized ashflows and for nonwelded ashflows with relatively high combined quartz and feldspar contents in UE-25a#1 and the base of the zone in USW G-2. Postdehydration behavior in the functional Tuffaceous Beds is also apparently complex, with coefficients of -4.5, +4.4, and $+7.8 \times 10^{-6}\ K^{-1}$ appropriate for nonwelded ashflows, for partially welded ashflows, and for bedded/reworked zones, respectively.

On cooling, the expansion behavior of these strongly zeolitized tuffs depends on the availability of water. If the tuffs are not rehydrated, they will contract continuously to ambient temperature, resulting in net contraction if they are dewatered on heating. If fully rehydrated, then behavior on cooling should be the reverse of that on heating and the final net volume change should be zero.

Data provided in this report are intended to serve largely as a basis for (1) near-field and/or very near-field thermomechanical modeling studies based on average properties, and (2) sensitivity analyses to be performed as part of evaluating potential repository horizons in tuff. The amount of data is limited in all areas. The approach taken, however, demonstrates a method by which other required functional stratigraphies can be developed.

APPENDIX

Detailed Data and Uncertainties in Picking the Upper and Lower Boundaries of the Functional Tuffaceous Beds

The upper and lower boundaries of the functional Tuffaceous Beds are picked here on the basis of data contained in (a) lithologic logs, (b) mineralogical analyses, (c) downhole density logs, and (d) bulk property analyses. In each hole, data both within the zone and near the upper and lower boundaries are described, as is the approximate uncertainty in the locations of the boundaries. The data are described in slightly abbreviated outline form to avoid excessive length. All detailed discussion is in terms of feet, since this is how all onsite drilling and coring records are kept.

A. Hole: USW G-1

Functional Interval: Tuffaceous Beds

Interval: Depths of from 1395 to 1865 ft (425.2 to 568.5 m; elevation 757.2 to 900.5 m)
(Note: Throughout, depths and elevations were not corrected for hole deviation. Unitless numbers are depths in feet. Sample numbers are equivalent to depth in feet.)

General Characteristics of Zone

- Lithologic log:[2] Nonwelded devitrified ashflow and bedded/reworked zone at base of Topopah Spring Member extend from 1394 to 1426 ft. Tuffaceous Beds of Calico Hills consist of five nonwelded ashflows, with thin bedded/reworked zones between flows. Lower 66 ft of unit (1736 to 1802 ft) is bedded/reworked zone, including tuffaceous sandstone. Prow Pass Member contains partially welded, devitrified ashflow between top of unit (1802) and 1867.

- Mineralogy:[3] Samples from 1400 to 1854 ft contain $\geq$30% clinoptilolite. Average clinoptilolite content 50 percent; mordenite absent. Except for Sample 1639, all contain negligible montmorillonite. Sample 1639 contains 10% to 20% clay.

- Downhole density log (Birdwell, noncompensated, no proximity index): Logged density is 1.8 to 1.9 g/cm^3 from 1395 to 1550 ft, decreasing to ~1.70 g/cm^3 at 1600 ft and gradually increasing to 1.9 g/cm^3 at 1750 ft. Bedded/reworked zone at base of Tuffaceous Beds of Calico Hills is irregularly higher in density, with maximum near 2.15 g/cm^3. Upper portion of Prow Pass Member is relatively uniform in bulk density near 1.9 g/cm^3 to 1865 ft. Because of lack of proximity index and compensation, logged density data are qualitative only.

- Bulk property data (Terra Tek, Inc., Salt Lake): Unit is subdivided here into three parts:

Upper Portion (1395 to 1736 ft)

- grain density (28 samples): 2.40±0.08 g/cm^3
- porosity: 0.36±0.03
- bulk density: 1.89±0.04 g/cm^3

Bedded/Reworked (1736 to 1802 ft)

- grain density (6 samples): 2.56±0.08 g/cm^3
- porosity: 0.30±0.06
- bulk density: 2.10±0.12 g/cm^3

Lower Ashflow (1802 to 1865 ft)

- grain density (4 samples): 2.41±0.04 g/cm^3
- porosity: 0.36±0.01
- bulk density: 1.90±0.02 g/cm^3

Note throughout that all reported bulk properties are accompanied by uncertainties. Previous work[10] indicates that grain densities of zeolitic tuffs should (conservatively) be precise to ±0.06 g/cm^3 at the 1-σ level of confidence, calculated bulk densities at 100% saturation to ±0.06 g/cm^3, and calculated porosities to ±0.06. Inherent variability within the functional Tuffaceous Beds and unavoidable uncertainty in bulk-property measurement and calculation dictate cautious consideration of averages and distributions of bulk properties reported here as only approximate.

<u>Top of Interval</u>: 1395 ft

<u>Data</u>

- Lithologic log:[2] Partially to nonwelded vitric ashflow 1361 to 1394 ft; nonwelded devitrified ashflow 1394 to 1404 ft.

- Mineralogy:[3] Sample 1392, 0.8 to 0.95 glass; Sample 1400, 0.6 to 0.9 clinoptilolite.

- Downhole density log: Continuous gradual decrease in density from 2.2 g/cm^3 at 1330 ft to 1.75 g/cm^3 at 1385 ft.

- Bulk property data: Grain density of 2.38 g/cm^3 in basal vitrophyre of Topopah Spring Member; no marked change with zeolitization. No data available from bedded/reworked zone at base of Topopah Spring Member.

Uncertainty: Based on mineralogy, +3, -5 ft elevation.

Bottom of Interval: 1865 ft

Data

- Lithologic log:[2] 1802 to 1867 ft, partially welded devitrified ashflow; 1867 to 1977 ft, partially to moderately welded, devitrified ashflow.

- Mineralogy:[3] Sample 1854, 0.26 to 0.40 clinoptilolite; Sample 1883, devitrified tuff, zeolite-free, clay-free.

- Downhole density log: Gradual increase in logged density from 1.81 g/cm^3 at 1830, to 2.04 g/cm^3 at 1900.

- Bulk property data: (grain density (g/cm^3), porosity): Sample 1847, 2.44, 0.37; Sample 1886, 2.59, 0.32; Sample 1927, 2.63, 0.32.

Uncertainty: +11, -18 ft, based on mineralogy.

B. Hole: UE-25a#1

Functional Interval: Tuffaceous Beds

Interval: Depths of from 1320 to 1845 ft (402.3 to 562.4 m, elevation 636.8 to 796.9 m)

General Characteristics of Zone

- Lithologic log:[17] Devitrified basal portion of Topopah Spring Member extends from 1325 to 1360 ft; bedded/reworked interval from 1360 to 1364 ft. Tuffaceous Beds of Calico Hills includes six ashflows and five thin bedded/reworked intervals, underlain by 47 ft of bedded/reworked tuff and tuffaceous sandstone (1789 to 1836 ft, base of unit). Upper 9 ft of Prow Pass Member (1836 to 1845 ft) in non- to partially welded ashflow.

- Mineralogy:[7] Samples from 1324 to 1824 ft all contain abundant zeolites (clinoptilolite and/or heulandite). Samples at 1279 ft (vitric) and 1852 ft (welded, devitrified) are nearly free of zeolites.

- Downhole density log (Birdwell, noncompensated, no proximity index): Logged density very irregular above 1350 ft, decreases from 2.0 g/cm^3 at 1350 ft to 1.85 g/cm^3 at 1390 ft. Density increases gradually to 2.05 g/cm^3 at 1500 ft, drops to 1.9 g/cm^3 at 1510 ft, and is fairly uniform near 1.85 g/cm^3 between 1600 and 1770 ft, from where it increases into bedded/reworked zone. Density is 2.05 to 2.3 g/cm^3 in bedded/reworked zone, lower in uppermost portion of Prow Pass Member.

- Bulk property data: Unit divides easily into three subunits. Data are available from several sources, including a US Geological Survey (USGS) open-file report,[19] and many bulk-property measurements at both Holmes and Narver and Terra Tek. Holmes and Narver data have been formally reported;[20] those from Terra Tek are unpublished. Data from Holmes and Narver and Terra Tek are considered together here as Sandia National Laboratory (SNL) data.

Average measured and calculated values follow:

Upper Portion (1320 to 1789 ft)

- grain density

USGS (12 samples):	2.32±0.07 g/cm^3
SNL (13 samples):	2.40±0.04 g/cm^3

- porosity
  - USGS: 0.30±0.04
  - SNL: 0.33±0.03

- bulk density
  - USGS: 1.93±0.06 g/cm^3
  - SNL: 1.94±0.04 g/cm^3

Bedded/Reworked (1789 to 1836 ft) (2 USGS samples only):

- grain density: 2.47 g/cm^3
- porosity: 0.20
- bulk density: 2.17 g/cm^3

Top of Interval: 1320 ft

Data

- Lithologic log:[17] Basal vitrophyre of Topopah Spring Member extends to 1317 ft, with vitric welded to 1325 ft; nonwelded to partially welded, devitrified ashflow extends from 1325 to 1340 ft.

- Mineralogy:[7] Sample 1323 contains abundant clinoptilolite. Sample 1279 predominantly glass with minor heulandite.

- Downhole density log: Sharp drop in density starts at 1290 ft, extends to 1330 ft, thin zone at 1340 to 1350 ft with density near 2.15 g/cm^3; then the density drops again.

- Bulk property data (grain density (g/cm^3), porosity): Sample 1591, 2.43, 0.14; Sample 1370, 2.36, 0.31.

Uncertainty: Pick based on combination of mineralogy and lithologic log; +0, -3 ft. Lithologic log and mineralogy are not completely consistent.

Bottom of Interval: 1845 ft

Data

- Lithologic log:[17] Upper Prow Pass Member described as devitrified ash flow; tuffaceous sandstones noted in bedded/reworked base of Tuffaceous Beds of Calico Hills; contact at 1845 ft.

- Mineralogy:[7] Sample 1824 is feldpathic litharenite, with abundant clay and some zeolite. Sample 1852 is predominantly quartz and feldspar. Litharenite is 10 ft thick. No data are available from the uppermost Prow Pass Member.

- Downhole density log: The high-density zone at the base of the Tuffaceous Beds of Calico Hills is tuffaceous sandstone (ρ_b = 2.3 g/cm^3); top of welded/devitrified Prow Pass Member is clearly visible at 1850 ft, with virtually no low-density zone at the top of the Member.

- Bulk property data (grain density (g/cm^3), porosity): Sample 1815, 2.47, 0.26; Sample 1866, 2.57, 0.29.

Uncertainty: Contact could be moved up to the base of the lowest ashflow, i.e., +47 ft; it can be moved downward only to the top of the devitrified Prow Pass Member, -5 ft. Very limited data available from bedded/reworked zone.

C. Hole: USW G-2

Functional Interval: Tuffaceous Beds

Interval: Depths of from 1680 to 2704 ft (512.1 to 824.2 m, elevation 729.7 to 1041.8 m)

General Characteristics of Zone

- Lithologic log:[21] Lower part of Topopah Spring Member includes partially to nonwelded, devitrified ashflow between 1681 and 1701 ft, bedded/reworked zone between 1701 and 1757 ft. Tuffaceous Beds of Calico Hills include 16 nonwelded ashflows, with thin bedded/reworked zones intervening. Unit is faulted out at 2704 ft; thus no basal bedded/reworked zone is present.

- Mineralogy:[8] Traces of zeolite occur in the Topopah Spring Member as shallow as 1536 ft. A "densely welded, devitrified" sample (1634) is rich in clinoptilolite, but above the basal vitrophyre of the Topopah Spring Member. Continuous zeolitization appears to begin at 1691 ft, with abundant clinoptilolite. Clinoptilolite and mordenite occur together to 2528 ft; mordenite alone at 2667 ft, the lowest sample taken in unit. Except for the lower Topopah Spring Member, smectite contents all are <0.05; the lower Topopah Spring Member contains 10% clay.

- Downhole density log (Birdwell, compensated): Logged density decreases from 2.2 to 1.95 g/cm^3 between 1660 and 1680 ft, then is $\leq$2.0 g/cm^3 to the base of the Topopah Spring Member at 1757 ft. Density of Tuffaceous Beds of Calico Hills is quite uniform at 1.8 to 1.9 g/cm^3 between 1770 and 2100 ft, 1.9 to 2.0 g/cm^3 between 2100 and 2570 ft. Between 2570 and 2600, density $\geq$2.0 g/cm^3. From 2600 to 2704 ft, the density gradually increases from 2.0 to 2.2 g/cm^3.

- Bulk property data: Unit is relatively homogeneous, treated as single zone. Averages of measured values (all from Terra Tek) are:
  - grain density (48 samples): 2.40±0.05 g/cm^3
  - porosity: 0.31±0.04
  - bulk density: 1.97±0.08 g/cm^3

Of the 48 samples analyzed, only two are from bedded/reworked zones.

Top of Interval: 1680 ft

Data

- Lithologic log:[21] Basal vitrophyre of Topopah Spring Member extends 1634-1664, moderately to densely welded vitric from 1664 to 1669 ft, moderately welded, vitric to devitrified from 1669 to 1681 ft.

- Mineralogy:[8] Sample 1664, 0.5 to 0.7 glass; Sample 1691, 0.45 to 0.7 clinoptilolite + mordenite.

- Downhole density log: Logged density decreases from 2.2 g/cm^3 at 1660 ft to 1.95 g/cm^3 at 1680 ft and is relatively constant below this depth.

- Bulk-property data: (grain density (g/cm^3), porosity): Sample 1664, 2.39, 0.07; Sample 1723, 2.37, 0.30.

Uncertainty: Contact picked largely on basis of break in density log, could be ±11 ft.

Bottom of Interval: 2704 ft

Data

- Lithologic log:[21] Fault picked at 2704 ft, faulting a thick nonwelded ashflow in Tuffaceous Beds of Calico Hills against densely welded Prow Pass Member.

- Mineralogy:[8] Sample 2677, 0.2 to 0.4 mordenite; Sample 2744 zeolite-free devitrified tuff.

- Downhole density log: Logged density increases sharply from 2.2 g/cm^3 at 2700 ft to 2.45 g/cm^3 at 2710 ft.

- Bulk property data: (grain density (g/cm^3), porosity): Sample 2700, 2.44, 0.21; Sample 2734, 2.52, 0.09.

<u>Uncertainty</u>: All data are consistent with the pick in the lithologic log. The only uncertainty would result from hole deviation from the vertical or from an incomplete core recovery.

REFERENCES

1. Johnstone, J. K., Peters, R. R., and Gnirk, P. F., 1984: Unit Evaluation at Yucca Mountain, Nevada Test Site: Summary Report and Recommendation; SAND83-0372, Sandia National Laboratories, Albuquerque, NM.

2. Spengler, R. W., Byers, F. M., Jr., and Warner, J. B., 1981: Stratigraphy and Structure of Volcanic Rocks in Drill Hole USW-G1, Yucca Mountain, Nye County, Nevada; Open-File Report 81-1349, U.S. Geological Survey, Denver, CO.

3. Waters, A. C., and Carroll, P. R., eds., 1981: Preliminary Stratigraphic and Petrologic Characterization of Core Samples from USW-G1, Yucca Mountain, Nevada; LA-8840-MS, Los Alamos National Laboratory, Los Alamos, NM.

4. Lappin, A. R., 1981: Thermal Conductivity of Silicic Tuffs: Predictive Formalism and Comparison With Preliminary Experimental Results; SAND80-0769, Sandia National Laboratories, Albuquerque, NM.

5. Olsson, W. A., and Jones, A. K., 1980: Rock Mechanics Properties of Volcanic Tuffs From the Nevada Test Site; SAND80-1453, Sandia National Laboratories, Albuquerque, NM.

6. Iman, R. L., Helton, J. C., and Campbell, J. E., 1978: Risk Methodology for Geologic Disposal of Radioactive Waste: Sensitivity Analysis Techniques; SAND78-0912, Sandia National Laboratories, Albuquerque, NM.

7. Sykes, M. L., Heiken, G. H., and Smyth, J. R., 1979: Mineralogy and Petrology of Tuff Units From the UE 25a-1 Drill Site, Yucca Mountain, Nevada; LA-8139-MS, Los Alamos National Laboratory, Los Alamos, NM.

8. Caporuscio, F., Vaniman, D., Bish, D., Broxton, D., Arney, B., Heiken, G., Byers, F., Gooley, R., and Semarge, E., 1982: Petrologic Studies of Drill Cores USW-G2, and UE 25b-1H, Yucca Mountain, Nevada; LA-9255-MS, Los Alamos National Laboratory, Los Alamos, NM.

9. Mumpton, F. A., ed., 1977: Mineralogy and Geology of Natural Zeolites; Mineralogical Society of America Short Course Notes, Vol. 4, Southern Printing Co., Blacksburg, VA.

10. Lappin, A. R., Van Buskirk, R. G., Ennis, D. O., Butters, S. W., Prater, F. M., Muller, C. S., and Bergosh, J. L., 1982: Thermal Conductivity, Bulk Properties, and Thermal Stratigraphy of Silicic Tuffs From the Upper Portion of Hole USW-G1, Yucca Mountain, Nye County, Nevada; SAND81-1873, Sandia National Laboratories, Albuquerque, NM.

11. Lappin, A. R., 1980: Preliminary Thermal Expansion Screening Data for Tuffs; SAND78-1147, Sandia National Laboratories, Albuquerque, NM.

12. Hoover, D. L., 1968: Genesis of Zeolites, Nevada Test Site; in E. B. Eckel, ed., Nevada Test Site, Geol. Soc. Amer. Memoir 110, pp. 275-284.

13. Ross, C. S., and Smith, R. L., 1955: Water and Other Volatiles in Volcanic Glasses; Amer. Mineral., V. 40, pp. 1071-1089.

14. White, A. F., 1979: Geochemistry of Ground Water Associated With Tuffaceous Rocks, Oasis Valley, Nevada; Prof. Pap 712-E, U.S. Geological Survey, Washington, DC.

15. Bish, D. L., 1981: Detailed Mineralogical Characterization of the Bullfrog and Tram Members in USW G-1, With Emphasis on Clay Mineralogy; LA-9021-MS, Los Alamos National Laboratory, Los Alamos, NM.

16. Breck, D. W., 1974: Zeolite Molecular Sieves; John Wiley and Sons, New York, 771 p.

17. Spengler, R. W., Muller, D. C., and Livermore, R. B., 1979: Preliminary Report on the Geology and Geophysics of Drill Hole UE25a-1, Yucca Mountain, Nevada Test Site; Open-File Report 79-1244, U.S. Geological Survey, Denver, CO.

18. Zimmerman, R. M., 1983: First Phase of Small Diameter Heater Experiments in Tuff; 24th U.S. Symposium Rock Mechanics, pp. 271-282.

19. Anderson, L. A., 1981: Rock Property Analysis of Core Samples from the Yucca Mountain UE25a-1 Borehole, Nevada Test Site, Nevada; Open-File Report 81-1338, U.S. Geological Survey, Denver, CO.

20. Yelamanchili, N. B. C., to Lappin, A. R., 12/13/78: Bulk Physical Properties of Tuffs From Hole UE25a-1; Holmes and Narver, Inc., NTS.

21. Maldonado, F., and Koether, S. L., 1983: Stratigraphy, Structure, and Some Petrographic Features of Tertiary Volcanic Rocks at the USW G-2 Drill Hole, Yucca Mountain, Nye County, Nevada; Open-File Report 83-732, U.S. Geological Survey, Denver, CO.

DISTRIBUTION LIST

B. C. Rusche (RW-1)
Director
Office of Civilian Radioactive
Waste Management
U.S. Department of Energy
Forrestal Building
Washington, DC 20585

J. W. Bennett (RW-22)
Office of Geologic Repositories
U.S. Department of Energy
Forrestal Building
Washington, DC 20585

Ralph Stein (RW-23)
Office of Geologic Repositories
U.S. Department of Energy
Forrestal Building
Washington, DC 20585

J. J. Fiore, (RW-22)
Program Management Division
Office of Geologic Repositories
U.S. Department of Energy
Forrestal Building
Washington, DC 20585

M. W. Frei (RW-23)
Engineering & Licensing Division
Office of Geologic Repositories
U.S. Department of Energy
Forrestal Building
Washington, DC 20585

E. S. Burton (RW-25)
Siting Division
Office of Geologic Repositories
U.S. Department of Energy
Forrestal Building
Washington, D.C. 20585

C. R. Cooley (RW-24)
Geosciences & Technology Division
Office of Geologic Repositories
U.S. Department of Energy
Forrestal Building
Washington, DC 20585

T. P. Longo (RW-25)
Program Management Division
Office of Geologic Repositories
U.S. Department of Energy
Forrestal Building
Washington, DC 20585

Cy Klingsberg (RW-24)
Geosciences and Technology Division
Office of Geologic Repositories
U. S. Department of Energy
Forrestal Building
Washington, DC 20585

B. G. Gale (RW-25)
Siting Division
Office of Geologic Repositories
U.S. Department of Energy
Forrestal Building
Washington, D.C. 20585

R. J. Blaney (RW-22)
Program Management Division
Office of Geologic Repositories
U.S. Department of Energy
Forrestal Building
Washington, DC 20585

R. W. Gale (RW-40)
Office of Policy, Integration, and
Outreach
U.S. Department of Energy
Forrestal Building
Washington, D.C. 20585

J. E. Shaheen (RW-44)
Outreach Programs
Office of Policy, Integration and
Outreach
U.S. Department of Energy
Forrestal Building
Washington, DC 20585

J. O. Neff, Manager
Salt Repository Project Office
U.S. Department of Energy
505 King Avenue
Columbus, OH 43201

D. C. Newton (RW-23)
Engineering & Licensing Division
Office of Geologic Repositories
U.S. Department of Energy
Forrestal Building
Washington, DC 20585

O. L. Olson, Manager
Basalt Waste Isolation Project Office
U.S. Department of Energy
Richland Operations Office
Post Office Box 550
Richland, WA 99352

D. L. Vieth, Director (4)
Waste Management Project Office
U.S. Department of Energy
Post Office Box 14100
Las Vegas, NV 89114

D. F. Miller, Director
Office of Public Affairs
U.S. Department of Energy
Post Office Box 14100
Las Vegas, NV 89114

D. A. Nowack (12)
Office of Public Affairs
U.S. Department of Energy
Post Office Box 14100
Las Vegas, NV 89114

B. W. Church, Director
Health Physics Division
U.S. Department of Energy
Post Office Box 14100
Las Vegas, NV 89114

Chief, Repository Projects Branch
Division of Waste Management
U.S. Nuclear Regulatory Commission
Washington, D.C. 20555

Document Control Center
Division of Waste Management
U.S. Nuclear Regulatory Commission
Washington, D.C. 20555

S. A. Mann, Manager
Crystalline Rock Project Office
U.S. Department of Energy
9800 South Cass Avenue
Argonne, IL 60439

K. Street, Jr.
Lawrence Livermore National
Laboratory
Post Office Box 808
Mail Stop L-209
Livermore, CA 94550

L. D. Ramspott (3)
Technical Project Officer for NNWSI
Lawrence Livermore National
Laboratory
P.O. Box 808
Mail Stop L-204
Livermore, CA 94550

W. J. Purcell (RW-20)
Office of Geologic Repositories
U.S. Department of Energy
Forrestal Building
Washington, DC 20585

D. T. Oakley (4)
Technical Project Officer for NNWSI
Los Alamos National Laboratory
P.O. Box 1663
Mail Stop F-671
Los Alamos, NM 87545

W. W. Dudley, Jr. (3)
Technical Project Officer for NNWSI
U.S. Geological Survey
Post Office Box 25046
418 Federal Center
Denver, CO 80225

NTS Section Leader
Repository Project Branch
Division of Waste Management
U.S. Nuclear Regulatory Commission
Washington, D.C. 20555

V. M. Glanzman
U.S. Geological Survey
Post Office Box 25046
913 Federal Center
Denver, CO 80225

P. T. Prestholt
NRC Site Representative
1050 East Flamingo Road
Suite 319
Las Vegas, NV 89109

M. E. Spaeth
Technical Project Officer for NNWSI
Science Applications
International, Corporation
2769 South Highland Drive
Las Vegas, NV 89109

SAIC-T&MSS Library (2)
Science Applications
International, Corporation
2950 South Highland Drive
Las Vegas, NV 89109

W. S. Twenhofel, Consultant
Science Applications
International, Corp.
820 Estes Street
Lakewood, CO 80215

A. E. Gurrola
General Manager
Energy Support Division
Holmes & Narver, Inc.
Post Office Box 14340
Las Vegas, NV 89114

J. A. Cross, Manager
Las Vegas Branch
Fenix & Scisson, Inc.
Post Office Box 15408
Las Vegas, NV 89114

N. E. Carter
Battelle Columbus Laboratory
Office of Nuclear Waste Isolation
505 King Avenue
Columbus, OH 43201

John Fordham
Desert Research Institute
Water Resources Center
Post Office Box 60220
Reno, NV 89506

J. B. Wright
Technical Project Officer for NNWSI
Westinghouse Electric Corporation
Waste Technology Services Division
Nevada Operations
Post Office Box 708
Mail Stop 703
Mercury, NV 89023

ONWI Library
Battelle Columbus Laboratory
Office of Nuclear Waste Isolation
505 King Avenue
Columbus, OH 43201

W. M. Hewitt, Program Manager
Roy F. Weston, Inc.
2301 Research Blvd., 3rd Floor
Rockville, MD 20850

H. D. Cunningham
General Manager
Reynolds Electrical &
Engineering Co., Inc.
Post Office Box 14400
Mail Stop 555
Las Vegas, NV 89114

T. Hay, Executive Assistant
Office of the Governor
State of Nevada
Capitol Complex
Carson City, NV 89710

R. R. Loux, Jr., Director (3)
Nuclear Waste Project Office
State of Nevada
Capitol Complex
Carson City, NV 89710

C. H. Johnson, Technical
Program Manager
Nuclear Waste Project Office
State of Nevada
Capitol Complex
Carson City, NV 89710

Dr. Martin Mifflin
Desert Research Institute
Water Resources Center
Suite 1
2505 Chandler Avenue
Las Vegas, NV 89120

Department of Comprehensive
Planning
Clark County
225 Bridger Avenue, 7th Floor
Las Vegas, NV 89155

Lincoln County Commission
Lincoln County
Post Office Box 90
Pioche, NV 89043

Community Planning and
Development
City of North Las Vegas
Post Office Box 4086
North Las Vegas, NV 89030

City Manager
City of Henderson
Henderson, NV 89015

N. A. Norman
Project Manager
Bechtel National Inc.
P. O. Box 3965
San Francisco, CA 94119

5163 D. F. McVey
5171 R. K. Thomas
6300 R. W. Lynch
6310 T. O. Hunter
6310 NNWSICF
6311 L. W. Scully
6311 L. Perrine (2)
6312 F. W. Bingham
6313 T. E. Blejwas
6313 F. B. Nimick (20)
6314 J. R. Tillerson
6314 S. J. Bauer
6314 B. Ehgartner
6314 M. Ford
6314 A. J. Mansure
6314 R. E. Stinebaugh
6315 S. Sinnock
6315 D. H. Zeuch
6331 A. R. Lappin (10)
6332 WMT Library (20)
6430 N. R. Ortiz
3141 C. M. Ostrander (5)
3151 W. L. Garner (3)
8024 M. A. Pound
DOE/TIC (28)
(3154-3, C. H. Dalin)

Planning Department
Nye County
Post Office Box 153
Tonopah, NV 89049

Economic Development
Department
City of Las Vegas
400 East Stewart Avenue
Las Vegas, NV 89101

Director of Community
Planning
City of Boulder City
Post Office Box 367
Boulder City, NV 89005

Commission of the
European Communities
200 Rue de la Loi
B-1049 Brussels
BELGIUM

R. Harig
Parsons Brinckerhoff Quade &
Douglas, Inc.
1625 Van Ness Ave.
San Francisco, CA 94109-3678

V. J. Cassella (RW-22)
Office of Geologic Repositories
U.S. Department of Energy
Forrestal Building
Washington, DC 20585

Technical Information Center
Roy F. Weston, Inc.
2301 Research Boulevard,
Third Floor
Rockville, MD 20850